The transition state and regulation of γ-TuRC-mediated microtubule nucleation revealed by single molecule microscopy

Akanksha Thawani[1], Michael J Rale[2], Nicolas Coudray[3], Gira Bhabha[3], Howard A Stone[4], Joshua W Shaevitz[5,6], Sabine Petry[2,*]

[1]Department of Chemical and Biological Engineering, Princeton University, Princeton NJ, USA

[2]Department of Molecular Biology, Princeton University, Princeton NJ, USA

[3]Department of Cell Biology, New York University School of Medicine, New York NY, USA

[4]Department of Mechanical and Aerospace Engineering, Princeton University, Princeton NJ, USA

[5]Lewis-Sigler Institute for Integrative Genomics and [6]Department of Physics, Princeton University, Princeton NJ, USA

* Correspondence: spetry@princeton.edu

Abstract

Determining how microtubules (MTs) are nucleated is essential for understanding how the cytoskeleton assembles. While the MT nucleator, γ-tubulin ring complex (γ-TuRC) has been identified, precisely how γ-TuRC nucleates a MT remains poorly understood. Here we developed a single molecule assay to directly visualize nucleation of a MT from purified *Xenopus laevis* γ-TuRC. We reveal a high γ-/αβ-tubulin affinity, which facilitates assembly of a MT from γ-TuRC. Whereas spontaneous nucleation requires assembly of 8 αβ-tubulins, nucleation from γ-TuRC occurs efficiently with a cooperativity of 4 αβ-tubulin dimers. This is distinct from pre-assembled MT seeds, where a single dimer is sufficient to initiate growth. A computational model predicts our kinetic measurements and reveals the rate-limiting transition where laterally-associated αβ-tubulins drive γ-TuRC into a closed conformation. Putative activation domain of CDK5RAP2, NME7 and TPX2 do not enhance γ-TuRC-mediated nucleation, while XMAP215 drastically increases the nucleation efficiency by strengthening the longitudinal γ-/αβ-tubulin interaction.

Introduction

Microtubules (MTs) enable cell division, motility, intracellular organization and transport. Half a century ago, MTs were found to be composed of αβ-tubulin dimers, yet how MTs are nucleated in the cell to assemble the cellular structures remains poorly understood[1,2]. The universal nucleator, γ-tubulin efficiently nucleates MTs *in vivo*[3–5] by forming a 2.2 megadalton, ring-shaped complex with γ-tubulin complex proteins (GCPs), known as the γ-Tubulin Ring Complex (γ-TuRC)[6–11]. Structural studies[9,12–15] have revealed that γ-TuRC positions a lateral array of 13 γ-tubulin molecules that are thought to template MT assembly by binding αβ-tubulin dimers and promoting their lateral interaction to result in nucleation of a MT[9,12,16–18]. Despite this model being widely accepted, MT nucleation from γ-TuRC molecules has not been directly visualized in real time and the dynamics of nucleation of a MT from αβ-tubulin dimers remains to be characterized. In particular, determining the critical nucleus, i.e., the rate-limiting transition state, for γ-TuRC nucleation is of tremendous interest, as it has important implications for how MT nucleation is spatiotemporally regulated in the cell (Fig. 1A).

In the absence of γ-TuRC, MTs can also nucleate spontaneously from high concentrations of αβ-tubulin *in vitro*. In this process, which displays a nucleation barrier, the assembly of many αβ-tubulin dimers is thought to occur to form lateral and longitudinal contacts[19–22]. It has long been speculated whether γ-TuRC-mediated nucleation occurs similarly, or follows a distinct reaction pathway[18,22–25]. Moreover, the structure of native γ-TuRC shows an *open* conformation where adjacent γ-tubulin do not form a lateral interaction[13–15], raising further questions on how the conformational mismatch impacts γ-TuRC's nucleation activity (Fig. 1A). It has been widely proposed that γ-TuRC may transition to a *closed* conformation during MT assembly to match the geometry of αβ-tubulin dimers arranged laterally in the MT lattice[10,13]. This transition could further

provide a mode of regulation through several putative MT-associated proteins (MAPs) that have been proposed to promote a closed conformation of γ-TuRC's[10,13,18] and regulate γ-TuRC's nucleation activity[9,10,13,26–28]. Finally, the interaction affinity between γ-tubulin and αβ-tubulin and its role on MT nucleation remain unknown[18,23] (Fig. 1A).

Investigating the molecular biophysics of MT nucleation by γ-TuRC at the single-molecule level and with computational modeling have the potential to address these questions. By identifying transition states and reaction intermediates during the γ-TuRC-mediated nucleation reaction, important insights into the dynamics of MT nucleation can be revealed. Yet, technical challenges in both purifying γ-TuRC at high yield, as well as the inability to visualize MT nucleation events from individual γ-TuRC molecules in real time and at high resolution, have posed limitations. In this work, we overcome these longstanding challenges to reconstitute MT nucleation from γ-TuRC and visualize the reaction live at the resolution of single molecules. We use computational models to gain further mechanistic insights into MT nucleation and to identify the molecular composition and arrangement of the rate-limiting transition state in γ-TuRC. Finally, we examine the roles of various MAPs, particularly the co-nucleation factor XMAP215, in γ-TuRC-mediated MT nucleation and comprehensively examine how specific biomolecular features govern how MT nucleation from γ-TuRC occurs.

Results

Visualizing microtubule nucleation from γ-TuRC with single molecule microscopy

To study how γ-TuRC nucleates a MT, we purified endogenous γ-TuRC from *Xenopus* egg extracts and biotinylated the complexes to immobilize them on functionalized glass (Fig. 1-figure supplement 1A-B). Upon perfusing fluorescent αβ-tubulin, we visualized MT nucleation live with total internal reflection fluorescence microscopy (TIRFM) (Fig. 1B). Strikingly, MT nucleation events occurred specifically from γ-TuRC molecules that were either unlabeled (Fig. 1B and Video 1) or fluorescently labelled during the purification (Fig. 1-figure supplement 1C and Video 2). Kymographs revealed that single, attached γ-TuRC molecules assembled αβ-tubulin into a MT *de novo* starting from zero length within the diffraction limit of light microscopy (Fig. 1C), ruling out an alternative model where MTs first spontaneously nucleate and then become stabilized via γ-TuRC. By observing fiduciary marks on the MT lattice (Fig. 1C) and generating polarity-marked MTs from attached γ-TuRC (Fig. 1- figure supplement 1D), we show that γ-TuRC caps the MT minus-end while only the plus-end polymerizes, as supported by previous works[16,17]. Notably, the detachment of γ-TuRC molecules and re-growth of the MT minus-ends were not observed, and γ-TuRC persists on the MT minus-end for the duration of our experiments. Altogether, our results demonstrate that γ-TuRC directly nucleates a MT.

Molecular composition of the transition state during γ-TuRC-mediated nucleation

To determine how γ-TuRC nucleates a MT, we measured the kinetics of MT nucleation for a constant density of γ-TuRC molecules and increasing αβ-tubulin concentrations (Fig. 2A and Video 3). γ-TuRCs nucleated MTs starting from 7 μM tubulin (Fig. 2A-B), which is higher than

the minimum tubulin concentration (*C**) needed for growth from a pre-formed MT plus-end (*C** = 1.4 μM, Fig. 2B). Furthermore, the number of MTs nucleated from γ-TuRC increased non-linearly with αβ-tubulin concentration as opposed to the linear increase in MT's growth speed with tubulin concentration (Fig. 2B). By measuring the number of MTs nucleated over time with varying αβ-tubulin concentration (Fig. 2C), we calculated the rate of MT nucleation. The power-law dependence on αβ-tubulin concentration (Fig. 2D) yields the number of tubulin dimers, 3.9 ± 0.5, that compose the rate-limiting, transition state during MT assembly from γ-TuRC (Fig. 2D). Thus, the cooperative assembly of nearly 4 αβ-tubulin subunits on γ-TuRC represents the most critical, rate-limiting step in MT nucleation.

γ-TuRC-mediated nucleation is more efficient than spontaneous nucleation

Based on the traditional assay where MTs are nucleated, fixed and visualized, a large variability in γ-TuRC's MT nucleation activity has been observed. With this setup, γ-TuRC has often been reported to be a poor nucleator with a similar activity as spontaneous MT nucleation[6,8–11,13,14,26,29]. With our live TIRFM assay, we aimed to quantitatively compare the efficiency of γ-TuRC-mediated MT nucleation with spontaneous MT nucleation (Fig. 3A). In contrast to γ-TuRC-mediated nucleation, a higher concentration of 14 μM tubulin was required for any spontaneous assembly of MTs, after which both the plus- and minus-ends polymerize (Fig. 3B, Fig. 3-figure supplement 1A and Video 4). The number of MTs assembled as a function of the αβ-tubulin concentration displayed a power-law dependence with an even larger exponent of 8.1 ± 0.9 (Fig. 3C), indicating a highly cooperative process that requires 8 αβ-tubulin dimers in a rate-limiting intermediate, in agreement with previous reports[19,20]. Further, direct comparison and measurement of spontaneous MT assembly with γ-TuRC-mediated nucleation (Fig. 3- figure supplement 1B-C)

115 clearly demonstrates that γ-TuRC nucleates MTs significantly more efficiently. Notably, specific
116 attachment of γ-TuRC to coverslips is also required to observe the nucleation activity (Fig. 3-
117 figure supplement 1C). In sum, γ-TuRC-mediated nucleation occurs efficiently and its critical
118 nucleus requires less than half the number of αβ-tubulin dimers compared to spontaneous
119 assembly.
120
121 **Contribution of end architecture of γ-TuRC to microtubule nucleation**
122 The MT plus-end architecture, which ranges from blunt to tapered, is critical for MT
123 polymerization dynamics[30–32], and was recently proposed to be critical for MT nucleation[25]. To
124 investigate how the blunt-end geometry of γ-TuRC contributes to its nucleation kinetics and
125 transition state, we generated Alexa-568 labelled, stable MT seeds with blunt ends as described
126 previously[25] and compared MT assembly from seeds upon addition of Cy5-labelled αβ-tubulin
127 dimers (Fig. 3C) side-by-side with γ-TuRC-mediated nucleation. At a minimum concentration of
128 2.45μM, approaching the critical concentration needed for polymerization of a MT plus-end, a
129 large proportion of pre-formed MT seeds assemble MTs (Fig. 3C-D, Fig. 3-figure supplement 1D
130 and Video 5). At 7 μM tubulin, the rate of assembly of MTs from the blunt seeds increased to reach
131 the maximum rate that could be temporally resolved, i.e. all of the MT seeds immediately
132 assembled a MT (Fig. 4D). This is in contrast to the kinetics of γ-TuRC-mediated nucleation at
133 7μM tubulin concentration, where minimal nucleation activity was observed (Fig. 2C-D). The
134 measured reaction kinetics as a function of the αβ-tubulin concentration (Fig. 3D) was used to
135 obtain the power-law of the nucleation rate, 1 ± 0.3 (Fig. 3E). This suggests that in our assay
136 condition, blunt MT ends assemble tubulin dimers into the MT lattice non-cooperatively. In other
137 words, the addition of a single αβ-tubulin dimer suffices to overcome the rate-limiting barrier,

which also occurs during the polymerization phase of MT dynamics. Notably, when this experiment was replicated with the coverslip preparation and assay conditions reported previously[25], a high concentration of tubulin was necessary for seeds to assemble MTs in agreement with the previous work[25]. However, our assay conditions, that were used to compare seed-templated MT assembly with γ-TuRC-mediated nucleation side-by-side, result in a low, minimal tubulin concentration that is needed for seed-mediated MT assembly. To conclude, while the γ-TuRC positions a blunt plus-end of γ-tubulins, the contribution of this specific end architecture in defining the kinetics of nucleation from γ-TuRC and its transition state is minimal.

In summary, because γ-TuRC positions an array of γ-tubulins at its nucleation interface that are thought to stabilize intrinsically weak, lateral αβ/αβ-tubulin interaction[9,10,13,14,18,22,23], MT nucleation by γ-TuRC has been proposed to function similar to polymerization of a MT end. Here we show several lines of evidence that γ-TuRC-mediated nucleation has distinct characteristics from MT polymerization and assembly from blunt MT seeds. While growth speed of MTs nucleated from γ-TuRC or templated from MT seeds is similar (Fig. 3-figure supplement 1D), γ-TuRC molecules do not nucleate MTs at low tubulin concentration where MT polymerization can occur. Further increasing tubulin concentration results in a non-linear increase in the number of γ-TuRCs molecules that nucleate MT, as opposed to a linear increase in rate of assembly from seeds. At the highest tubulin concentrations, approximately 10-15% of γ-TuRCs nucleate MTs in the TIRF assays. While these results were obtained with endogenous γ-TuRCs purified from cytosol, it remains possible that specific factors at MTOCs can modulate γ-TuRC's conformation and kinetics. In summary, the rate-limiting transition state on γ-TuRC is composed of four αβ-tubulin dimers in contrast with MT polymerization where one tubulin dimer suffices to overcome the slowest step.

161

162 **γ-tubulin has a high affinity for αβ-tubulin**

163 Consequently, specific biochemical features of γ-TuRC must govern its nucleation activity and the
164 composition of the transition state during nucleation. To address this, we first measured the
165 interaction affinity between γ-tubulin and αβ-tubulin, which could provide insight into γ-TuRC's
166 nucleation interface and its role in MT nucleation. To begin, we performed size-exclusion
167 chromatography where γ-tubulin alone elutes as a broad peak in fractions I-N (Fig. 4A (i), pseudo-
168 colored profile in green) at low concentration. Interestingly, in the presence of either 10 μM (low)
169 or 35 μM (high) concentrations of αβ-tubulin, the γ-tubulin binds to αβ-tubulin (pseudo-colored
170 profile in cyan) and elutes earlier, specifically in fraction H (Fig. 4A (ii-iii), yellow arrow). Further,
171 the overall elution profile of γ-tubulin is altered to follow αβ-tubulin, showing that γ-tubulin binds
172 to αβ-tubulin at both the low and high concentrations we tested. To compare this with αβ-/αβ-
173 tubulin's longitudinal interaction, we performed chromatography of αβ-tubulin alone (Fig. 4-
174 figure supplement 1A). At a lower concentration (10μM), αβ-tubulin elutes only as a single subunit
175 in fractions H-K (Fig. 4-figure supplement 1A (i)). Only at high αβ-tubulin concentration (35μM)
176 did we detect a small population of αβ-tubulin bound to another αβ-tubulin (Fig. 4-figure
177 supplement 1A (i), fractions B-C denoted with red arrows). This suggests that the heterogeneous
178 γ-/αβ-tubulin affinity is higher than the αβ-/αβ-tubulin.

179 To further investigate how γ-tubulin and αβ-tubulin interact, we turned to single molecule
180 microscopy. We attached biotinylated αβ-tubulin dimers to a coverslip, added either fluorescently-
181 labelled αβ-tubulin (Fig. 4B(i)) or γ-tubulin (Fig. 4B(ii)) to the solution, and visualized the binding
182 of single fluorescent molecules to αβ-tubulin molecules on the coverslip. While both fluorescent
183 αβ-tubulin and γ-tubulin specifically bind to surface-attached αβ-tubulin, 15-fold more γ-tubulin

184 molecules were bound than αβ-tubulin molecules (Fig. 4C), further supporting a stronger γ-/αβ-
185 tubulin interaction. Finally, these results were confirmed with a biolayer interferometry assay,
186 where lower concentrations of γ-tubulin were detected to interact with probe-bound αβ-tubulin,
187 while a much higher concentration of αβ-tubulin was necessary to measure an interaction between
188 αβ-/αβ-tubulin dimers (Fig. 4-figure supplement 1B). These results are congruent with *in vivo* γ-
189 /αβ-tubulin affinity measurements made in yeast cells[33].

190 In performing the above experiments, we unexpectedly found that purified γ-tubulin on its
191 own, at high concentrations and at 33 °C, efficiently nucleated MTs from αβ-tubulin subunits (Fig.
192 4-figure supplement 2A) and capped MT minus-ends while allowing plus-ends to polymerize (Fig.
193 4-figure supplement 2B). Besides its ability to form higher order oligomers in a physiological
194 buffer[29], γ-tubulin at high concentrations also forms filaments *in vitro* of variable widths (Fig. 4-
195 figure supplement 2C; Moritz and Agard, unpublished results) as assayed by negative stain
196 electron microscopy (EM). The formation of filaments *in vitro* is consistent with the previous *in*
197 *vivo* observations where γ-tubulin was over-expression and immunoprecipited[34–36]. To understand
198 the nature of these filaments, we generated 3D reconstructions, which revealed that γ-tubulins self-
199 assemble into lateral arrays with a repeating unit of approximately 54Å (Fig. 4-figure supplement
200 2D-E). This closely matches the lateral tubulin repeats in the MT lattice (PDB:6DPU[37,38]) and in
201 γ-tubulin crystal contacts (52Å, PDB:1Z5W[39,40]), but not the longitudinal αβ-tubulin repeat (40Å).
202 This suggests that laterally associated γ-tubulin are sufficient to efficiently nucleate MTs.

203 In sum, at the nucleation interface of γ-TuRC, γ-tubulin has a higher longitudinal affinity
204 for αβ-tubulin compared to αβ-tubulin's affinity for itself, which promotes MT nucleation from γ-
205 TuRC.

206

Monte Carlo simulations recapitulate the dynamics microtubule nucleation from γ-TuRC

To further probe the dynamics of MT nucleation, we developed Monte Carlo simulations to model MT nucleation from γ-TuRC. Our model was based on one previously developed for the plus-end dynamics of a MT[31,41,42]. A 13-protofilament geometry for the MT lattice and γ-TuRC were used with a pitch of 3 tubulins (Fig. 5A). αβ-tubulin dimers arrive with a constant on rate, k_{on} ($\mu M^{-1}s^{-1}$) on each protofilament. The interactions between αβ-tubulins was assumed to occur with longitudinal and lateral bond energies, $\Delta G_{Long,\alpha\beta-\alpha\beta}$ and $\Delta G_{Lat,\alpha\beta-\alpha\beta}$, respectively, similar to previous literature[31,41,42]. The longitudinal bond energy between γ-/αβ-tubulin, $\Delta G_{Long,\gamma-\alpha\beta}$ determines the dwell time of αβ-tubulin dimers on γ-TuRC. An open conformation of native γ-TuRC was assumed, as observed in recent structural work[13,14], where lateral interactions between tubulins on neighboring sites were not allowed. A thermodynamic barrier, $\Delta G_{\gamma TuRC-conf}$ and a pre-factor rate constant $k_{\gamma TuRC-conf}$ (s^{-1}) determine the transition from this open to *closed* γ-TuRC conformation where lateral tubulin interactions can occur (Fig. 5A). As αβ-tubulin dimers assemble on γ-TuRC, the free energy of this transition decreases by the total energy of all n lateral bonds that can be formed, $\Delta G_{\gamma TuRC-conf} - n\Delta G_{Lat,\alpha\beta-\alpha\beta}$.

MT growth parameters were determined by fitting to experimental growth speed curves (Fig. 5-figure supplement 1A), and were found to be similar to previous estimates[31,41]. Based on our biochemical measurement (Fig. 4), $\Delta G_{Long,\gamma-\alpha\beta}$ was estimated to be higher than $\Delta G_{Long,\alpha\beta-\alpha\beta}$, while a wide range was explored for the other parameters. The resulting model produces a sharp transition from zero-MT length to a continuously growing MT upon γ-TuRC closure (Fig. 5B) that occurs at variable time points for each realization of the model (Fig. 5B and Fig. 5-figure supplement 1B-C(i)). This qualitatively recapitulates the dynamics of γ-TuRC-mediated nucleation events observed experimentally.

Nucleation kinetics and the power-law dependence on αβ-tubulin concentration was obtained by simulating hundreds of model realizations. While $k_{\gamma TuRC-conf}$ and $\Delta G_{Long,\gamma-\alpha\beta}$ do not alter the power-law exponent significantly, they set the rate of nucleation at a specific αβ-tubulin concentration (Fig. 5-figure supplement 1B-C). The thermodynamic barrier, $\Delta G_{\gamma TuRC-conf}$ instead determines the power-law exponent and the number of αβ-tubulins in the rate-limiting, transition state (Fig. 5C). At $\Delta G_{\gamma TuRC-conf} < 2.5 k_B T$, cooperative assembly of 1-2 αβ-tubulins suffice to nucleate MTs, while at high $\Delta G_{\gamma TuRC-conf} > 20 k_B T$, more than 5 αβ-tubulins assemble cooperatively for successful MT nucleation. At an intermediate $\Delta G_{\gamma TuRC-conf} = 10 k_B T$, MT nucleation kinetics and its power-law dependence recapitulates our experimental measurements (compare Fig. 5-figure supplement 2A with Fig. 2C-D). Here γ-TuRCs minimally nucleate MTs at 7μM tubulin, MT nucleation increases non-linearly with tubulin concentration, and 4 ± 0.4 αβ-tubulins compose the transition state (Fig. 5-figure supplement 2A and Fig. 5C, green curve highlighted with an asterisk).

As a further validation of our model, we simulated the dynamics of MT nucleation from blunt MT seeds. Here we assumed that MT assembly begins from a closed γ-TuRC geometry where all longitudinal bond energies were set equal to $\Delta G_{Long,\alpha\beta-\alpha\beta}$ (Fig. 5-figure supplement 2B). The simulations predict near complete MT assembly at minimal αβ-tubulin concentration of 2μM and transition state of 1.1 ± 0.1 αβ-tubulins (Fig. 5-figure supplement 2B), in agreement with MT assembly from blunt seeds that we measured experimentally (Fig. 3D-E). Thus, our Monte Carlo simulations accurately capture the detailed dynamics of MT nucleation from γ-TuRC.

Arrangement of αβ-tubulin dimers in transition state for γ-TuRC-mediated microtubule nucleation

We next characterized the dynamics of αβ-tubulins during MT nucleation from γ-TuRC by examining the time traces from individual model simulations. First, prior to MT nucleation, we observe longitudinal association of individual αβ-tubulins either to the γ-tubulin sites on the open γ-TuRC or, less frequently, with existing αβ-tubulin in a protofilament (Fig. 5B, left insets). These αβ-tubulins dissociate rapidly in the absence of additional lateral bond energy. Once a MT lattice is assembled, persistence of αβ-tubulin dimers with both longitudinal and lateral contacts drive the growth of plus-end. Analogous observations during growth of a MT plus-end also show rapid dissociation of αβ-tubulin that form only a longitudinal contact, while ones with additional lateral contacts persist[31]. At the sharp transition prior to MT assembly (Fig. 5B, right insets), we find that many αβ-tubulin dimers stochastically assemble on neighboring sites on γ-TuRC. Favorable Gibbs free energy from the lateral interaction between these αβ-tubulin dimers overcomes the energy penalty of the conformational change and transitions γ-TuRC into a closed state.

Finally, we characterize the arrangement of αβ-tubulin dimers in the rate-limiting, transition state that results in a closed γ-TuRC conformation prior to MT polymerization. A variable total number of αβ-tubulin dimers with an average of 5.2 ± 1 (n=2119 simulations) were present on γ-TuRC at the transition state (Fig. 5D, left). To our surprise, αβ-tubulin subunits in the transition state assemble on neighboring sites into laterally-arranged groupings (Fig. 5D, right). The most probable transition state is composed of four αβ-tubulin arranged on neighboring sites that form 3 lateral bonds when the γ-TuRC conformation changes to a closed one. The other probable states have 5 αβ-tubulins arranged laterally in two groups of 2 and 3 dimers each, or in two groups of 1 and 4 dimers each, and 6 αβ-tubulins arranged in two groups of 2 and 4 dimers, or in two groups of 3 dimers each. Most importantly, in these transition states, the free energy gained from the lateral bonds between αβ-tubulins compensates for the thermodynamic barrier posed by γ-TuRC's

276 open conformation to allow for MT nucleation. Notably, the laterally-arranged group of 4 αβ-
277 tubulin dimers physically represents the power-law exponent measured from the average
278 nucleation kinetics (Fig. 2D).
279
280 **Role of putative activation factors in γ-TuRC mediated nucleation**
281 Next, we investigated how accessory factors regulate γ-TuRC-dependent MT nucleation. While
282 several activation factors[26,27,43] have been proposed to enhance the MT nucleation activity of γ-
283 TuRC, the function of these putative activation factors remains to be tested with a sensitive and
284 direct assay. We incubated the purified γ-TuRC activation domain (γ-TuNA)[26] from *Xenopus*
285 *laevis* protein CDK5RAP2 with γ-TuRC at high concentrations to maximally saturate the binding
286 sites on γ-TuRC (Fig. 6A), and further supplemented additional γ-TuNA with αβ-tubulin used
287 during the nucleation assay. Measurement of nucleation activity revealed that CDK5RAP2's γ-
288 TuNA domain increases γ-TuRC-mediated nucleation only by 1.4 (± 0.02) -fold (mean ± std, n =
289 2) at t = 180 seconds, falling within the 95% confidence intervals of the control reactions (Fig. 6A-
290 B and Video 6). Another putative activator, NME7[27], when added to γ-TuRC at saturating
291 concentrations[44] (Fig. 6-figure supplement 1 and Video 6), did not increase γ-TuRC's nucleation
292 activity (Fig. 6B). Finally, we assessed the protein TPX2 that not only contains a split γ-TuNA and
293 overlapping SPM[43], but also functions as an anti-catastrophe factor *in vitro*[25,45] and was proposed
294 to stimulate γ-TuRC-mediated nucleation[43,46,47]. TPX2 also had a small increase on the nucleation
295 activity of γ-TuRC by 1.2 (± 0.3) -fold (mean ± std, n = 3) at t = 180 seconds, but bound strongly
296 along the MT lattice (Fig. 6C-D and Video 6). While high concentration of TPX2 forms
297 condensates with αβ-tubulin and promotes spontaneous MT nucleation[45,48], near its endogenous
298 concentration of TPX2[49] used here, TPX2 is able to saturates the MT lattice, yet it does not

299 significantly increase γ-TuRC-mediated nucleation, in agreement with the physiological
300 observations[43]. Thus, the putative activation motif of CDK5RAP2, full-length NME7 or TPX2 all
301 have minor effects on γ-TuRC's MT nucleation activity.
302
303 **XMAP215 promotes microtubule nucleation by strengthening the longitudinal bond energy**
304 **between γ-TuRC and αβ-tubulin**
305 Recently, XMAP215 was discovered to be a nucleation factor that synergizes with γ-TuRC in *X.*
306 *laevis* and *S. cerevisiae*[29,50], or works in an additive manner with γ-tubulin[51]. To investigate how
307 XMAP215 participates in MT nucleation, we performed single molecule experiments with
308 XMAP215 and γ-TuRC. At low tubulin concentrations of 3.5μM and 7μM, where none or little
309 MT nucleation occurs from γ-TuRCs alone (Fig. 7A and Fig. 7-figure supplement 1A), as shown
310 earlier. Strikingly, the addition of XMAP215 induced many surface-attached γ-TuRCs to nucleate
311 MTs, resulting in a drastic increase in number of nucleated MTs by 25 (±9) -fold (mean ± std, n =
312 3) within t = 120 seconds (Fig. 7A-B, Fig. Fig. 7-figure supplement 1B and Video 7). By directly
313 visualizing γ-TuRC and XMAP215 molecules during the nucleation reaction (Fig. 7C), we found
314 that XMAP215 and γ-TuRC molecules first form a complex from which a MT was then nucleated
315 (Fig. 7C and Video 8). For 76% of the events (n=56), XMAP215 visibly persisted between 3 to
316 ≥300 seconds on γ-TuRC before MT nucleation. After MT nucleation, XMAP215 molecules
317 polymerize and track with the MT plus-end. For 50% of nucleation events (n=58), some
318 XMAP215 molecules remained on the minus-end together with γ-TuRC, while for the other 50%
319 of events, XMAP215 was not observed on the minus-end after nucleation. This suggests that
320 XMAP215 molecules nucleate with γ-TuRC and then continue polymerization of the plus-end.

How does XMAP215 enable MT nucleation from γ-TuRC? We titrated αβ-tubulin at constant γ-TuRC and XMAP215 concentrations and measured the kinetics of nucleation (Fig. 7-figure supplement 1C and Fig. 7D). XMAP215 effectively decreases the minimal tubulin concentration necessary for MT nucleation from γ-TuRC to 1.6μM (Fig. 7-figure supplement 1C), very close to the minimal concentration for plus-end polymerization. As before, we calculated the composition of the transition state by measuring the power-law dependence between the MT nucleation rate and tubulin concentration with a resulting cooperative assembly of 3.3 ± 0.8 αβ-tubulin dimers occurs (Fig. 7E). This suggests that XMAP215 does not lower the thermodynamic barrier to nucleation by altering the geometry of γ-TuRC. Further, neither the N-terminus, containing TOG1-4 domains, nor the C-terminus of XMAP215, containing the TOG5 and C-terminal domain that directly interact with γ-tubulin[29], stimulate additional nucleation from γ-TuRC (Fig. 7-figure supplement 1D-E).

Finally, we used our simulations to understand the thermodynamics underlying the MT nucleation activity of XMAP215. Based on its role in accelerating both MT polymerization and nucleation[29,50], we implicitly modeled the thermodynamic effect of XMAP215's activity by strengthening the longitudinal tubulin bonds, as described previously[41]. The simulation where only the longitudinal αβ-/αβ-tubulin bond is strengthened does not capture the enhancement of MT nucleation by XMAP215 (Fig. 7D, left). Instead, simulations where both the longitudinal γ-/αβ-tubulin and αβ-/αβ-tubulin bond energies are increased by 1.2-fold captures the accelerated kinetics of MT nucleation at low αβ-tubulin concentrations. These simulations also predict a similar transition state composition as measured experimentally (Fig. 7D-E, left), supporting XMAP215's role in strengthening γ-/αβ-tubulin interactions at the nucleation interface. Altogether, our results confirm that XMAP215 indeed functions synergistically with γ-TuRC, in

agreement with recent works[15,29,50]. Most importantly, our results show that, while the transition state is defined by γ-TuRC's conformation, XMAP215 strengthens the longitudinal γ-/αβ-tubulin bond to function as a bona-fide nucleation factor.

Inhibition of γ-TuRC mediated nucleation by specific microtubule associated proteins

Finally, we asked whether specific MAPs could have an inhibitory effect on MT nucleation from γ-TuRC. The two most abundant inhibitory MAPs in the cytosol, MCAK and Stathmin function by removing αβ-tubulin dimers from the MT lattice[52,53] or sequestering αβ-tubulin dimers[54,55], respectively. We find that addition of either sub-endogenous concentration of MCAK, or near-endogenous Stathmin concentration (Fig. 7F, Fig. 7-figure supplement 2 and Video 9) was sufficient to nearly abolish MT nucleation from all γ-TuRC molecules. Thus, γ-TuRC-mediated nucleation is inhibited by MAPs that inhibit MT polymerization.

Discussion

Decades after the discovery of MTs, their αβ-tubulin subunits and the identification of γ-TuRC as the universal MT nucleator[3,6–8,16,17], it has remained poorly understood how MTs are nucleated and how this process is regulated in the cell[18,22,46]. Here we establish a single-molecule assay to study MT nucleation and combine it with computational modelling to identify the rate-limiting, transition state of γ-TuRC-mediated nucleation . We examine how biochemical features of γ-TuRC contribute to its the nucleation activity and regulation.

New methods and direct measurements developed in this study reconcile several prior observations for γ-TuRC-mediated MT nucleation. First, the nucleation activity of γ-TuRC has been found as variable and often low and similar to spontaneous MT assembly[6,8,10,13–15,18,22], and γ-TuRC's requirement in the cell has been debated[4,45,56–58]. Low concentration of γ-TuRC molecules obtained from endogenous purifications and lack of live observation of a growing or capped MT minus-end, which is needed to distinguish between γ-TuRC-mediated and spontaneous nucleation, could affect the assessment of γ-TuRC's nucleation activity. Second, because of technical challenges in the traditional setup where MTs are nucleated, fixed and spun down onto a coverslip[6,8–10,13,26,27,29], variable assessment of the role of accessory factors[13,26,27] has been reported. Here, by developing a high resolution assay that provides specific live information to visualize MT nucleation events from γ-TuRC and distinguish between non-γ-TuRC nucleated MTs, analyses system to measure its nucleation activity independent of concentration, as well as direct visualization of MAPs bound to γ-TuRC or the MT lattice allows us to unambiguously study γ-TuRC mediated nucleation and its regulation by MAPs.

While the molecular architecture of γ-TuRC was revealed by recent cryo-EM structures[9,13–15], the dynamics of MT nucleation from γ-TuRC and how it relates to γ-TuRC's specific

biochemical features has remained unknown. By combining biochemical investigation with computational modeling, we show that 4 αβ-tubulin heterodimers on neighboring sites form the critical nucleus, i.e. the rate-limiting transition state on γ-TuRC. A model, in which γ-TuRC stochastically changes its conformation from an *open* to *closed* state, where the latter is stabilized by lateral αβ-tubulin interactions, comprehensively explains our experimental measurements. While native γ-TuRC purified from cytosol was used here, further activated γ-TuRC isolated from MTOCs may result in cooperativity between fewer αβ-tubulin dimers for successful nucleation. Likewise, MT assembly from pre-assembled, blunt seeds, could resemble nucleation from already closed γ-TuRCs. We find that the subsequent transition of the growing MT end from blunt- to tapered one, is not the major, rate-limiting step during nucleation from γ-TuRC. Notably, a parallel work also reported MT nucleation from single, human γ-TuRC molecules recently[15]. While the majority of findings agree with our work, 6.7 dimers were required in the critical nucleus and an overall lower activity of γ-TuRC (0.5%) was found[15]. Low structural integrity of purified γ-TuRC from incorporation of BFP-tagged GCP2 and a higher ratio of γ-tubulin sub-complexes, or species-specific variation in γ-TuRC properties could explain these differences.

Our simulations further predict that a hypothetical low affinity between γ-/αβ-tubulin[23] is insufficient to induce any MT nucleation because αβ-tubulins that bind to γ-TuRC dissociate rapidly. Instead, our biochemical investigation show that the high affinity of γ-/αβ-tubulin interaction increases the dwell time of αβ-tubulin dimers on γ-TuRC and promotes γ-TuRC's MT nucleation activity, as predicted by our modeling. Finally, this net mechanism is thermodynamically favorable compared to spontaneous MT nucleation as the free energy of longitudinal γ-/αβ-tubulin interactions, $13(\Delta G_{Long,\gamma-\alpha\beta})$, exceeds the energy penalty from conformational rearrangement of γ-TuRC, $\Delta G_{\gamma TuRC-conf}$. In sum, building on the recent structural

work[13–15], our results show that the open γ-TuRC conformation and its transition to a closed one defines γ-TuRC's nucleation activity and transition state. In the future, it will be important to study how γ-TuRC transitions to a closed conformation with high resolution structural studies, as well as how other biochemical properties, in addition to those modeled here, govern its nucleation activity. Our single molecule assay, kinetic analyses and computational modeling will be essential to complement and place atomic structures into a mechanism that explains how MT nucleation γ-TuRC occurs and how it is regulated.

Whereas spatial regulation of MT nucleation is achieved by localizing γ-TuRC to specific MTOC as shown previously[18,24,46,59], temporal regulation of MT nucleation had been proposed to occur through activation factors that modify γ-TuRC's conformation and upregulate its activity[18,26,27,46,59]. While several putative activation factors do not significantly enhance of γ-TuRC's nucleation activity as shown here, new factors, that are yet to be identified, may serve this role to alter γ-TuRC's conformation at MTOCs. Alternatively, we postulate another mechanism for temporal control governing the availability and localization of αβ-tubulin. In this model, locally concentrating soluble αβ-tubulin could upregulate the levels of γ-TuRC-mediated MT nucleation, e.g. as recently shown through accumulation of high concentration of tubulin dimers at the centrosome by MAPs[58,60] and by co-condensation of tubulin on MTs by TPX2 during branching MT nucleation[48], and finally via specific recruitment of tubulin on γ-TuRC through the binding of XMAP215 as shown here[29,50].

Supplementary Materials

Supplementary Materials includes nine figures, nine videos, MATLAB code for simulations and source data.

Acknowledgements

We thank Brian Mahon and Sophie Travis for advice on processing of electron microscopy data, David Agard, Michelle Moritz and Petry lab members for discussions. This work was supported by an American Heart Association predoctoral fellowship 17PRE33660328 and a Princeton University Honorific Fellowship (both to AT), a Howard Hughes Medical Institute Gilliam fellowship and a National Science Foundation graduate research fellowship (both to MJR), NIGMS R00GM112982 (to GB), NIH New Innovator Award 1DP2GM123493, Pew Scholars Program in the Biomedical Sciences 00027340, David and Lucile Packard Foundation 2014-40376 (all to SP), and the Center for the Physics of Biological Function sponsored by the National Science Foundation grant PHY-1734030.

Competing financial interests

The authors declare no competing financial interests.

Abbreviations List

Microtubule (MT)

Microtubule associated protein (MAP)

Gamma-tubulin (γ-tubulin) and Gamma-tubulin ring complex (γ-TuRC)

Gamma-tubulin complex protein (GCP)

444 Microtubule organizing center (MTOC)

445 Protofilament (pf)

446 Electron microscopy (EM)

References

1. Petry, S. Mechanisms of Mitotic Spindle Assembly. *Annu. Rev. Biochem.* **85**, 659–683 (2016).
2. Wu, J. & Akhmanova, A. Microtubule-Organizing Centers. *Annu. Rev. Cell Dev. Biol.* **33**, 51–75 (2017).
3. Oakley, C. E. & Oakley, B. R. Identification of gamma-tubulin, a new member of the tubulin superfamily encoded by mipA gene of Aspergillus nidulans. *Nature* **338**, 662–664 (1989).
4. Hannak, E. *et al.* The kinetically dominant assembly pathway for centrosomal asters in Caenorhabditis elegans is gamma-tubulin dependent. *J. Cell Biol.* **157**, 591–602 (2002).
5. Groen, A. C., Maresca, T. J., Gatlin, J. C., Salmon, E. D. & Mitchison, T. J. Functional overlap of microtubule assembly factors in chromatin-promoted spindle assembly. *Mol. Biol. Cell* **20**, 2766–2773 (2009).
6. Moritz, M., Braunfeld, M. B., Sedat, J. W., Alberts, B. & Agard, D. A. Microtubule nucleation by gamma-tubulin-containing rings in the centrosome. *Nature* **378**, 638–640 (1995).
7. Moritz, M., Zheng, Y., Alberts, B. M. & Oegema, K. Recruitment of the gamma-tubulin ring complex to Drosophila salt-stripped centrosome scaffolds. *J. Cell Biol.* **142**, 775–786 (1998).
8. Zheng, Y., Wong, M. L., Alberts, B. & Mitchison, T. Nucleation of microtubule assembly by a gamma-tubulin-containing ring complex. *Nature* **378**, 578–583 (1995).
9. Kollman, J. M., Polka, J. K., Zelter, A., Davis, T. N. & Agard, D. A. Microtubule nucleating gamma-TuSC assembles structures with 13-fold microtubule-like symmetry. *Nature* **466**, 879–882 (2010).
10. Kollman, J. M. *et al.* Ring closure activates yeast γTuRC for species-specific microtubule nucleation. *Nat. Struct. Mol. Biol.* **22**, 132–137 (2015).

11. Oegema, K. *et al.* Characterization of two related Drosophila gamma-tubulin complexes that differ in their ability to nucleate microtubules. *J. Cell Biol.* **144**, 721–733 (1999).
12. Moritz, M., Braunfeld, M. B., Guénebaut, V., Heuser, J. & Agard, D. A. Structure of the gamma-tubulin ring complex: a template for microtubule nucleation. *Nat. Cell Biol.* **2**, 365–370 (2000).
13. Liu, P. *et al.* Insights into the assembly and activation of the microtubule nucleator γ-TuRC. *Nature* **578**, 467–471 (2020).
14. Wieczorek, M. *et al.* Asymmetric Molecular Architecture of the Human γ-Tubulin Ring Complex. *Cell* **180**, 165-175.e16 (2020).
15. Consolati, T. *et al.* Microtubule Nucleation Properties of Single Human γTuRCs Explained by Their Cryo-EM Structure. *Dev. Cell* (2020) doi:10.1016/j.devcel.2020.04.019.
16. Keating, T. J. & Borisy, G. G. Immunostructural evidence for the template mechanism of microtubule nucleation. *Nat. Cell Biol.* **2**, 352–357 (2000).
17. Wiese, C. & Zheng, Y. A new function for the gamma-tubulin ring complex as a microtubule minus-end cap. *Nat. Cell Biol.* **2**, 358–364 (2000).
18. Kollman, J. M., Merdes, A., Mourey, L. & Agard, D. A. Microtubule nucleation by γ-tubulin complexes. *Nat. Rev. Mol. Cell Biol.* **12**, 709–721 (2011).
19. Voter, W. A. & Erickson, H. P. The kinetics of microtubule assembly. Evidence for a two-stage nucleation mechanism. *J. Biol. Chem.* **259**, 10430–10438 (1984).
20. Flyvbjerg, H., Jobs, E. & Leibler, S. Kinetics of self-assembling microtubules: an 'inverse problem' in biochemistry. *Proc. Natl. Acad. Sci. U.S.A.* **93**, 5975–5979 (1996).
21. Portran, D., Schaedel, L., Xu, Z., Théry, M. & Nachury, M. V. Tubulin acetylation protects long-lived microtubules against mechanical ageing. *Nat. Cell Biol.* **19**, 391–398 (2017).

22. Roostalu, J. & Surrey, T. Microtubule nucleation: beyond the template. *Nat. Rev. Mol. Cell Biol.* **18**, 702–710 (2017).

23. Rice, L., Moritz, M. & Agard, D. A. *Microtubules form by progressively faster tubulin accretion, not by nucleation-elongation*. http://biorxiv.org/lookup/doi/10.1101/545236 (2019) doi:10.1101/545236.

24. Wiese, C. & Zheng, Y. Microtubule nucleation: gamma-tubulin and beyond. *J. Cell. Sci.* **119**, 4143–4153 (2006).

25. Wieczorek, M., Bechstedt, S., Chaaban, S. & Brouhard, G. J. Microtubule-associated proteins control the kinetics of microtubule nucleation. *Nat. Cell Biol.* **17**, 907–916 (2015).

26. Choi, Y.-K., Liu, P., Sze, S. K., Dai, C. & Qi, R. Z. CDK5RAP2 stimulates microtubule nucleation by the gamma-tubulin ring complex. *J. Cell Biol.* **191**, 1089–1095 (2010).

27. Liu, P., Choi, Y.-K. & Qi, R. Z. NME7 is a functional component of the γ-tubulin ring complex. *Mol. Biol. Cell* **25**, 2017–2025 (2014).

28. Lynch, E. M., Groocock, L. M., Borek, W. E. & Sawin, K. E. Activation of the γ-tubulin complex by the Mto1/2 complex. *Curr. Biol.* **24**, 896–903 (2014).

29. Thawani, A., Kadzik, R. S. & Petry, S. XMAP215 is a microtubule nucleation factor that functions synergistically with the γ-tubulin ring complex. *Nat. Cell Biol.* **20**, 575–585 (2018).

30. Gardner, M. K. *et al.* Rapid Microtubule Self-Assembly Kinetics. *Cell* **159**, 215 (2014).

31. Mickolajczyk, K. J., Geyer, E. A., Kim, T., Rice, L. M. & Hancock, W. O. Direct observation of individual tubulin dimers binding to growing microtubules. *Proc. Natl. Acad. Sci. U.S.A.* **116**, 7314–7322 (2019).

514 32. Brouhard, G. J. & Rice, L. M. Microtubule dynamics: an interplay of biochemistry and
515 mechanics. *Nat. Rev. Mol. Cell Biol.* **19**, 451–463 (2018).
516 33. Erlemann, S. *et al.* An extended γ-tubulin ring functions as a stable platform in microtubule
517 nucleation. *J. Cell Biol.* **197**, 59–74 (2012).
518 34. Lindström, L. & Alvarado-Kristensson, M. Characterization of gamma-tubulin filaments in
519 mammalian cells. *Biochim Biophys Acta Mol Cell Res* **1865**, 158–171 (2018).
520 35. Chumová, J. *et al.* γ-Tubulin has a conserved intrinsic property of self-polymerization into
521 double stranded filaments and fibrillar networks. *Biochim Biophys Acta Mol Cell Res* **1865**,
522 734–748 (2018).
523 36. Pouchucq, L., Lobos-Ruiz, P., Araya, G., Valpuesta, J. M. & Monasterio, O. The chaperonin
524 CCT promotes the formation of fibrillar aggregates of γ-tubulin. *Biochimica et Biophysica*
525 *Acta (BBA) - Proteins and Proteomics* **1866**, 519–526 (2018).
526 37. Zhang, R., LaFrance, B. & Nogales, E. Separating the effects of nucleotide and EB binding
527 on microtubule structure. *Proc. Natl. Acad. Sci. U.S.A.* **115**, E6191–E6200 (2018).
528 38. Zhang, R. & Nogales, E. 6DPU: Undecorated GMPCPP microtubule. *Protein Data Bank:*
529 *www.rcsb.org/structure/6DPU* (2018) doi:10.2210/pdb6DPU/pdb.
530 39. Aldaz, H., Rice, L. M., Stearns, T. & Agard, D. A. Insights into microtubule nucleation from
531 the crystal structure of human gamma-tubulin. *Nature* **435**, 523–527 (2005).
532 40. Aldaz, H., Rice, L. M., Stearns, T. & Agard, D. A. 1Z5W: Crystal Structure of gamma-
533 tubulin bound to GTP. *Protein Data Bank: www.rcsb.org/structure/1Z5W* (2005)
534 doi:10.2210/pdb1Z5W/pdb.
535 41. VanBuren, V., Odde, D. J. & Cassimeris, L. Estimates of lateral and longitudinal bond
536 energies within the microtubule lattice. *Proc. Natl. Acad. Sci. U.S.A.* **99**, 6035–6040 (2002).

42. Ayaz, P. *et al.* A tethered delivery mechanism explains the catalytic action of a microtubule polymerase. *Elife* **3**, e03069 (2014).

43. Alfaro-Aco, R., Thawani, A. & Petry, S. Structural analysis of the role of TPX2 in branching microtubule nucleation. *J. Cell Biol.* **216**, 983–997 (2017).

44. Wühr, M. *et al.* Deep proteomics of the Xenopus laevis egg using an mRNA-derived reference database. *Curr. Biol.* **24**, 1467–1475 (2014).

45. Roostalu, J., Cade, N. I. & Surrey, T. Complementary activities of TPX2 and chTOG constitute an efficient importin-regulated microtubule nucleation module. *Nat. Cell Biol.* **17**, 1422–1434 (2015).

46. Tovey, C. A. & Conduit, P. T. Microtubule nucleation by γ-tubulin complexes and beyond. *Essays Biochem.* **62**, 765–780 (2018).

47. Zhang, R., Roostalu, J., Surrey, T. & Nogales, E. Structural insight into TPX2-stimulated microtubule assembly. *Elife* **6**, (2017).

48. King, M. R. & Petry, S. Phase separation of TPX2 enhances and spatially coordinates microtubule nucleation. *Nat Commun* **11**, 270 (2020).

49. Thawani, A., Stone, H. A., Shaevitz, J. W. & Petry, S. Spatiotemporal organization of branched microtubule networks. *Elife* **8**, (2019).

50. Gunzelmann, J. *et al.* The microtubule polymerase Stu2 promotes oligomerization of the γ-TuSC for cytoplasmic microtubule nucleation. *Elife* **7**, (2018).

51. King, B. R. *et al. XMAP215 and γ-tubulin additively promote microtubule nucleation in purified solutions*. http://biorxiv.org/lookup/doi/10.1101/2020.05.21.109561 (2020) doi:10.1101/2020.05.21.109561.

559 52. Hunter, A. W. *et al.* The kinesin-related protein MCAK is a microtubule depolymerase that
560 forms an ATP-hydrolyzing complex at microtubule ends. *Mol. Cell* **11**, 445–457 (2003).
561 53. Howard, J. & Hyman, A. A. Microtubule polymerases and depolymerases. *Curr. Opin. Cell*
562 *Biol.* **19**, 31–35 (2007).
563 54. Jourdain, L., Curmi, P., Sobel, A., Pantaloni, D. & Carlier, M. F. Stathmin: a tubulin-
564 sequestering protein which forms a ternary T2S complex with two tubulin molecules.
565 *Biochemistry* **36**, 10817–10821 (1997).
566 55. Belmont, L. D. & Mitchison, T. J. Identification of a protein that interacts with tubulin
567 dimers and increases the catastrophe rate of microtubules. *Cell* **84**, 623–631 (1996).
568 56. Rogers, G. C., Rusan, N. M., Peifer, M. & Rogers, S. L. A multicomponent assembly
569 pathway contributes to the formation of acentrosomal microtubule arrays in interphase
570 Drosophila cells. *Mol. Biol. Cell* **19**, 3163–3178 (2008).
571 57. Raff, J. W. Phase Separation and the Centrosome: A Fait Accompli? *Trends Cell Biol.* **29**,
572 612–622 (2019).
573 58. Woodruff, J. B. *et al.* The Centrosome Is a Selective Condensate that Nucleates Microtubules
574 by Concentrating Tubulin. *Cell* **169**, 1066-1077.e10 (2017).
575 59. Petry, S. & Vale, R. D. Microtubule nucleation at the centrosome and beyond. *Nat. Cell Biol.*
576 **17**, 1089–1093 (2015).
577 60. Baumgart, J. *et al.* Soluble tubulin is significantly enriched at mitotic centrosomes. *J. Cell*
578 *Biol.* **218**, 3977–3985 (2019).
579 61. Tan, S., Kern, R. C. & Selleck, W. The pST44 polycistronic expression system for producing
580 protein complexes in Escherichia coli. *Protein Expr. Purif.* **40**, 385–395 (2005).

581 62. Ohi, R., Sapra, T., Howard, J. & Mitchison, T. J. Differentiation of cytoplasmic and meiotic
582 spindle assembly MCAK functions by Aurora B-dependent phosphorylation. *Mol. Biol. Cell*
583 **15**, 2895–2906 (2004).
584 63. Reber, S. B. *et al.* XMAP215 activity sets spindle length by controlling the total mass of
585 spindle microtubules. *Nat. Cell Biol.* **15**, 1116–1122 (2013).
586 64. Hannak, E. & Heald, R. Investigating mitotic spindle assembly and function in vitro using
587 Xenopus laevis egg extracts. *Nat Protoc* **1**, 2305–2314 (2006).
588 65. Murray, A. W. & Kirschner, M. W. Cyclin synthesis drives the early embryonic cell cycle.
589 *Nature* **339**, 275–280 (1989).
590 66. Bieling, P., Telley, I. A., Hentrich, C., Piehler, J. & Surrey, T. Fluorescence microscopy
591 assays on chemically functionalized surfaces for quantitative imaging of microtubule, motor,
592 and +TIP dynamics. *Methods Cell Biol.* **95**, 555–580 (2010).
593 67. Thévenaz, P., Ruttimann, U. E. & Unser, M. A pyramid approach to subpixel registration
594 based on intensity. *IEEE Trans Image Process* **7**, 27–41 (1998).
595 68. Zanic, M. Measuring the Effects of Microtubule-Associated Proteins on Microtubule
596 Dynamics In Vitro. *Methods Mol. Biol.* **1413**, 47–61 (2016).
597 69. Le Maire, M., Aggerbeck, L. P., Monteilhet, C., Andersen, J. P. & Møller, J. V. The use of
598 high-performance liquid chromatography for the determination of size and molecular weight
599 of proteins: a caution and a list of membrane proteins suitable as standards. *Anal. Biochem.*
600 **154**, 525–535 (1986).
601 70. Ovesný, M., Křížek, P., Borkovec, J., Svindrych, Z. & Hagen, G. M. ThunderSTORM: a
602 comprehensive ImageJ plug-in for PALM and STORM data analysis and super-resolution
603 imaging. *Bioinformatics* **30**, 2389–2390 (2014).

604 71. Punjani, A., Rubinstein, J. L., Fleet, D. J. & Brubaker, M. A. cryoSPARC: algorithms for
605 rapid unsupervised cryo-EM structure determination. *Nat. Methods* **14**, 290–296 (2017).
606 72. Zhang, K. Gctf: Real-time CTF determination and correction. *J. Struct. Biol.* **193**, 1–12
607 (2016).
608 73. Pettersen, E. F. *et al.* UCSF Chimera--a visualization system for exploratory research and
609 analysis. *J Comput Chem* **25**, 1605–1612 (2004).
610

Methods

Purification of recombinant proteins

Full-length TPX2 with N-terminal Strep II-6xHis-GFP-TEV site tags was cloned into pST50Tr-STRHISNDHFR (pST50) vector[61] using Gibson Assembly (New England Biolabs). N-terminal 6xHis-tagged, *Xenopus laevis* Stathmin 1A was a gift from Christiane Wiese (University of Madison). N-terminal tagged 6xHis-TEV MCAK plasmid was a gift from Ryoma Ohi[62]. Wild-type XMAP215 with C-terminal GFP-7xHis plasmid was a gift from Simone Reber[63] and was used to clone XMAP215 with C-terminal SNAP-TEV-7xHis-StrepII tags as well as with C-terminal TEV-GFP-7xHis-StrepII tags, first into pST50 vector and further into pFastBac1 vector. TOG5-CT truncation of XMAP215 was produced by cloning amino acids 1091-2065 into pST50 vector with C-terminal GFP-7xHis-Strep tags. Human γ-tubulin TEV-Strep II-6xHis tags was codon-optimized for Sf9 expression, synthesized (Genscript), and further cloned into pFastBac1 vector. 6xHis tagged γ-TuNA (N-terminal aa 56-89 of *Xenopus laevis* CDK5RAP2) was also cloned into pST50 and expressed in *E. coli* Rosetta2 cells. Dual StrepII-6xHis-tagged *Xenopus laevis* NME7 was cloned into pFastBac1 vector, expressed, and purified from Sf9 cells.

TPX2, Stathmin and truncations of XMAP215 (TOG5-CT and TOG1-4) used in this study were expressed in *E. coli* Rosetta2 cells (EMD Millipore) by inducing with 0.5-1 mM IPTG for 12-18 hours at 16°C or 7 hours at 25°C. Wild-type XMAP215, MCAK and γ-tubulin were expressed and purified from Sf9 cells using Bac-to-Bac system (Invitrogen). The cells were lysed (EmulsiFlex, Avestin) and *E. coli* lysate was clarified by centrifugation at 13,000 rpm in Fiberlite F21-8 rotor (ThermoFisher) and Sf9 cell lysate at 50,000 rpm in Ti70 rotor (Beckman Coulter) for 30-45 minutes.

TPX2 was first affinity purified using Ni-NTA beads in binding buffer (50mM Tris-HCl pH 8.0, 750mM NaCl, 15mM Imidazole, 2.5mM PMSF, 6mM BME) and eluted with 200mM Imidazole. All protein was pooled and diluted 4-fold to 200mM final NaCl. Nucleotides were removed with a Heparin column (HiTrap Heparin HP, GE Healthcare) by binding protein in 250mM NaCl and isocratic elution in 750mM NaCl, all solutions prepared in Heparin buffer (50mM Tris-HCl, pH 8.0, 2.5mM PMSF, 6mM BME). Peak fractions were pooled and loaded on to Superdex 200 pg 16/600, and gel filtration was performed in CSF-XB buffer.

XMAP215-GFP-7xHis was purified using His-affinity (His-Trap, GE Healthcare) by binding in buffer (50mM $NaPO_4$, 500mM NaCl, 20mM Imidazole, pH 8.0) and eluting in 500mM Imidazole. Peak fractions were pooled and diluted 5-fold with 50mM Na-MES pH 6.6, bound to a cation-exchange column (Mono S 10/100 GL, GE Healthcare) with 50mM MES, 50mM NaCl, pH 6.6 and eluted with a salt-gradient up to 1M NaCl. Peak fractions were pooled and dialyzed into CSF-XB buffer. XMAP215-SNAP-TEV-7xHis-StrepII or XMAP215-TEV-GFP-7xHis-StrepII was first affinity purified with StrepTrap HP (GE Healthcare) with binding buffer (50mM $NaPO_4$, 270mM NaCl, 2mM $MgCl_2$, 2.5mM PMSF, 6mM BME, pH 7.2), eluted with 2.5mM D-desthiobiotin. Peak fractions were pooled, concentrated and further purification via gel filtration (Superdex 200 10/300 GL) in CSF-XB buffer containing 150mM KCl. For fluorescent labelling of SNAP-tag in XMAP215-SNAP-TEV-7xHis-StrepII, StrepTrap elution was cation-exchanged (Mono S 10/100 GL), peak fractions pooled and reacted with 2-molar excess SNAP-substrate Alexa-488 dye (S9129, NEB) overnight at 4°C, followed by purification via gel filtration (Superdex 200 10/300 GL) in CSF-XB buffer. Approximately 70% labeling efficiency of the SNAP-tag was achieved.

γ-tubulin was purified by binding to HisTrap HP (GE Healthcare) in binding buffer (50 mM KPO_4 pH 8.0, 500 mM KCl, 1 mM $MgCl_2$, 10% glycerol, 5mM Imidazole, 0.25 μM GTP, 5 mM BME, 2.5mM PMSF), washing first with 50 mM KPO_4 pH 8.0, 300 mM KCl, 1 mM $MgCl_2$, 10% glycerol, 25 mM imidazole, 0.25 μM GTP, 5 mM BME), and then with 50 mM K-MES pH 6.6, 500 mM KCl, 5mM $MgCl_2$, 10% glycerol, 25 mM imidazole, 0.25 μM GTP, 5 mM BME) and eluted in 50 mM K-MES pH 6.6, 500 mM KCl, 5mM $MgCl_2$, 10% glycerol, 250 mM imidazole, 0.25 μM GTP, 5 mM BME. Peak fractions were further purified with gel filtration (Superdex 200 10/300 GL) in gel filtration buffer (50 mM K-MES pH 6.6, 500 mM KCl, 5 mM $MgCl_2$, 1 mM K-EGTA, 1 μM GTP, 1 mM DTT). For covalent labelling of γ-tubulin with Alexa-568 or Alexa-488 dye, peak gel filtration fractions were pooled and dialyzed into labelling buffer (50mM KPO_4 pH 8.0, 500mM KCl, 1mM MgCl2, 2% glycerol, 25μM GDP, 5mM BME), reacted with 5 to 20-fold excess of Alexa-568 or Alexa-488 NHS ester (catalog # A20003, A20000, GE Healthcare) for 1 hour at 4°C, and unreacted dye was separated with size exclusion Superdex 200 10/300 GL in gel filtration buffer as above. 7% labelling of γ-tubulin was achieved.

γ-TuNA motif from CDK5RAP2 was purified by binding to Ni-NTA resin in binding buffer buffer (50mM Tris-HCl pH 8, 500mM NaCl, 20mM Imidazole), eluted with 250 mM Imidazole and further purified by gel filtration into storage buffer (50mM Tris-HCl pH 7.5, 200mM NaCl). NME7 was purified similar to γ-TuNA by first Ni-NTA affinity followed by size exclusion, as described for γ-TuNA, except with salt concentration of 150mM NaCl and additional 0.05% Tween-20, and further dialyzed into BRB80 for storage.

MCAK was first affinity purified by binding to His-Trap HP (GE Healthcare) in binding buffer (50mM NaPO4, 500mM NaCl, 6mM BME, 0.1mM MgATP, 10mM Imidazole, 1mM MgCl2, 2.5mM PMSF, 6mM BME, pH to 7.5), eluting with 300mM Imidazole, followed by gel-

679 filtration (Superdex 200 10/300 GL, GE Healthcare) in storage buffer (10 mM K-HEPES pH 7.7,
680 300 mM KCl, 6mM BME, 0.1 mM MgATP, 1mM $MgCl_2$, 10% w/v sucrose).
681 Stathmin was purified using His-affinity (His-Trap HP, GE Healthcare) by first binding in
682 binding buffer (20mM $NaPO_4$ pH 8.0, 500mM NaCl, 30mM Imidazole, 2.5mM PMSF, 6mM
683 BME) and eluting with 300mM Imidazole, followed by gel filtration (HiLoad 16/600 Superdex,
684 GE Healthcare) into CSF-XB buffer (100mM KCl, 10mM K-HEPES, 5mM K-EGTA, 1mM
685 $MgCl_2$, 0.1mM $CaCl_2$, pH 7.7 with 10% w/v sucrose).
686 All recombinant proteins were flash-frozen and stored at -80°C, and their concentration
687 was determined by analyzing a Coomassie-stained SDS-PAGE against known concentration of
688 BSA (A7906, Sigma).
689 Bovine brain tubulin was labelled with biotin-, Cy5-, Alexa-488 or Alexa-568 NHS esters
690 (GE Healthcare) as described previously[49].
691
692 **Purification, biotinylated and fluorescent labeling of γ-TuRC**
693 Endogenous γ-TuRC was purified from *Xenopus* egg extracts and labeled with the following steps
694 at 4°C. 7-8 ml of meiotic extract from *Xenopus* laevis eggs, prepared as described previously[64,65],
695 was first diluted 5-fold with CSF-XBg buffer (10mM K-HEPES, 100mM KCl, 1mM $MgCl_2$, 5mM
696 K-EGTA, 10% w/v sucrose, 1mM DTT, 1mM GTP, 10 µg/ml LPC protease inhibitors, pH 7.7),
697 centrifuged to remove large aggregates at 3500 rpm (Thermo Sorvall Legend XTR) for 10 minutes,
698 and the supernatant filtered sequentially with 1.2 µm and 0.8 µm Cellulose Acetate filters
699 (Whatman) followed by 0.22 µm PES filter (ThermoFisher). γ-TuRC was precipitated by
700 incubating with 6.5% w/v PEG-8000k (Sigma) for 30 minutes and centrifuged at 17,000 rpm (SS-
701 34 rotor, ThermoScientific) for 20 minutes. γ-TuRC-rich pellet was resuspended in CSF-XB buffer

with 0.05% v/v NP-40 using a mortar & pestle homogenizer, PEG was removed via centrifugation at 136,000 xg for 7 minutes in TLA100.3 (Beckman Ultracentrifuge), and supernatant was pre-cleared by incubating with Protein A Sepharose beads (GE LifeSciences #17127901) for 20 minutes. Beads were removed, γ-TuRC was incubated with 4-5 mg of a polyclonal antibody custom-made against C-terminal residues 413-451 of *X. laevis* γ-tubulin (Genscript) for 2 hours on gentle rotisserie, and further incubated with 1ml washed Protein A Sepharose bead slurry for 2 hours. γ-TuRC-bound beads were washed sequentially with 30 ml of CSF-XBg buffer, 30 ml of CSF-XBg buffer with 250 mM KCl (high salt wash), 10 ml CSF-XBg buffer with 5mM ATP (removes heat-shock proteins), and finally 10 ml CSF-XBg buffer before labeling. For biotinylation of γ-TuRC, beads were incubated with 25 μM NHS-PEG4-biotin (A39259, ThermoFisher) in CSF-XBg buffer for 1 hour at 4°C, and unbound biotin was removed by washing with 30 ml CSF-XBg buffer prior to elution step. For combined fluorescent and biotin labeling of γ-TuRC, the wash step after ATP-wash consisted of 10 ml of labelling buffer (10mM K-HEPES, 100mM KCl, 1mM $MgCl_2$, 5mM K-EGTA, 10% w/v sucrose, 0.5mM TCEP, 1mM GTP, 10 μg/ml LPC, pH 7.1) and fluorescent labelling was performed by incubating the beads with 1 μM Alexa-568 C_5 Maleimide (A20341, ThermoFisher). Unreacted dye was removed with 10 ml CSF-XBg buffer, beads were incubated with 25 μM NHS-PEG4-biotin (A39259, ThermoFisher) in CSF-XBg buffer for 1 hour at 4°C, and unreacted biotin removed with 30 ml CSF-XBg buffer. Labeled γ-TuRC was eluted by incubating 2-3ml of γ-tubulin peptide (residues 413-451) at 0.4-0.5mg/ml in CSF-XBg buffer with beads overnight. After 10-12 hours, γ-TuRC was collected by adding 1-2ml CSF-XBg buffer to the column, concentrated to 200 μl in 30k NMWL Amicon concentrator (EMD Millipore) and layered onto a continuous 10-50 w/w % sucrose gradient prepared in a 2.2 ml ultra-clear tube (11x34 mm, Beckman Coulter) using a two-step program in Gradient Master

725 108 machine. Sucrose gradient fractionation of γ-TuRC was performed by centrifugation at
726 200,000xg in TLS55 rotor (Beckman Coulter) for 3 hours. The gradient was fractionated from the
727 top in 11-12 fractions using wide-bore pipette tips and peak 2-3 fractions were identified by
728 immunoblotting against γ-tubulin with GTU-88 antibody (Sigma). γ-TuRC was concentrated to 80
729 µl in 30k NMWL Amicon concentrator (EMD Millipore) and fresh purification was used
730 immediately for single molecule assays. Cryo-preservation of γ-TuRC molecules resulted in loss
731 of ring assembly and activity.
732
733 **Assessment of γ-TuRC with protein gel, immunoblot and negative stain electron microscopy**
734 To assess the purity of γ-TuRC, 3-5 µl of purified γ-TuRC was visualized on an SDS-PAGE with
735 SYPRO Ruby stain (ThermoFisher) following the manufacturer's protocol. Biotinylated subunits
736 of γ-TuRC were assessed by immunoblotting with Streptavidin-conjugated alkaline phosphatase
737 (S921, ThermoFisher). For further conjugation of Alexa-568 dye to γ-TuRC, fluorescently labelled
738 subunits were assessed by visualizing an SDS-PAGE gel with Typhoon FLA 9500 (GE
739 Healthcare) with LPG filter and 100 µm pixel size. γ-TuRC purification was also assessed by
740 visualizing using electron microscopy. 4 µl of peak sucrose gradient fraction of γ-TuRC was
741 pipetted onto CF400-Cu grids (Electron Microscopy Sciences), incubated at room temperature for
742 60 seconds and then wicked away. 2% uranyl acetate was applied to the grids for 30 seconds,
743 wicked away, and the grids were air-dried for 10 minutes. The grids were imaged using Phillips
744 CM100 TEM microscope at 64000x magnification.
745
746 **Preparation of functionalized coverslips**

747 22x22 mm, high precision coverslips (170±5 μm, Carl Zeiss, catalog # 474030-9020-000) were
748 functionalized for single molecule assays based on a recent protocol[45,66] with specific
749 modifications. Briefly, coverslips were labelled on the surface to be functionalized by scratching
750 "C" on right, bottom corner, placed in Teflon racks, sonicated with 3N NaOH for 30 minutes,
751 rinsed with water and sonicated in piranha solution (2 parts of 30 w/w % hydrogen peroxide and
752 3 parts sulfuric acid) for 45 minutes. Coverslips were rinsed thrice in water, and all water was
753 removed by spin drying completely in a custom-made spin coater. Pairs of coverslips were made
754 to sandwich 3-glycidyloxypropyl trimethoxysilane (440167, Sigma) on the marked sides, placed
755 in glass petri dishes, and covalent reaction was performed in a lab oven at 75°C for 30 minutes.
756 Coverslips were incubated for 15 minutes at room temperature, the sandwiches were separated,
757 incubated in acetone for 15 minutes, then transferred to fresh acetone and quickly dried under
758 nitrogen stream. Coverslip sandwiches were prepared with a small pile of well mixed HO-PEG-
759 NH_2 and 10% biotin-CONH-PEG-NH_2 (Rapp Polymere) in glass petri dishes, warmed to 75°C in
760 the lab oven until PEG melts, air bubbles were pressed out and PEG coupling was performed at
761 75°C overnight. The following day, individual coverslips were separated from sandwiches,
762 sonicated in MilliQ water for 30 minutes, washed further with water until no foaming is visible,
763 dried with a spin dryer, and stored at 4°C. Functionalized coverslips were used within 1 month of
764 preparation.

765 Imaging chambers were prepared by first assembling a channel on glass slide with double
766 sided tape strips (Tesa) 5 mm apart, coating the channel with 2mg/ml PLL(20)-g[3.5]- PEG(2)
767 (SuSOS) in dH_2O, incubating for 20 minutes, rinsing out the unbound PEG molecules with dH_2O
768 and drying the glass slide under the nitrogen stream. A piece of functionalized coverslip was cut

with the diamond pen and assembled functionalized face down on imaging chamber. The prepared chambers were stored at 4°C and used within a day of assembly.

Microtubule nucleation assay with purified γ-TuRC

The imaging channel was prepared as follows. First, 5% w/v Pluronic F-127 in dH_2O was introduced in the chamber (1 vol = 50 µl) and incubated for 10 minutes at room temperature. The chamber was washed with 2 vols of assay buffer (80mM K-PIPES, 1mM $MgCl_2$, 1mM EGTA, 30mM KCl, 0.075% w/v methylcellulose 4000 cp, 1% w/v D-(+)-glucose, 0.02% w/v Brij-35, 5mM BME, 1mM GTP) with 0.05 mg/ml κ-casien (casein buffer), followed by 1 vol of 0.5 mg/ml NeutrAvidin (A2666, ThermoFisher) in casein buffer, incubated on a cold block for 3 minutes, and washed with 2 vols of BRB80 (80mM K-PIPES, 1mM $MgCl_2$, 1mM EGTA pH 6.8). 5-fold dilution of γ-TuRC in BRB80 was introduced in the flow chamber and incubated for 10 minutes. Unattached γ-TuRC molecules were washed with 1 vol of BRB80.

During the incubations, nucleation mix was prepared containing desired concentration of αβ-tubulin (3.5-21 µM) purified from bovine brain with 5% Cy5-labeled tubulin along with 1mg/ml BSA (A7906, Sigma) in assay buffer, centrifuged for 12 minutes in TLA100 (Beckman Coulter) to remove aggregates, a final 0.68 mg/ml glucose oxidase (SERVA, catalog # SE22778), 0.16 mg/ml catalase (Sigma, catalog # SRE0041) was added, and reaction mixture was introduced into the flow chamber containing γ-TuRC.

Total internal reflection fluorescence (TIRF) microscopy and analysis of microtubule nucleation from γ-TuRC

Nucleation of MTs was visualized with inverted Nikon TiE TIRF microscope using a 100X, 1.49 NA TIRF objective. An objective heater collar was attached (Bioptechs, model 150819-13) and the temperature set-point of 33.5°C was used for experiments. Time-lapse videos were recorded for 10 minutes at 0.5-1 frame per second using Andor iXon DU-897 camera with EM gain of 300 and exposure time of 50-200 ms each frame. Reference time-point zero (0 seconds) refers to when the reaction was incubated at 33.5°C on the microscope, and for most reactions, imaging was started within 30 seconds.

Growth speed of the plus-ends of MTs nucleated by γ-TuRC was measured by generating kymographs in ImageJ. For few specific datasets with notable in-plane drift, an ImageJ plugin, StackReg[67], was to correct a minor translational drift before proceeding with the analysis. Region of interest (ROI) for individual MTs were selected and resliced to generate a length-time plot and a line was fit to the growing MT plus-end. The slope of this line represents growth speed. The kinetics of MT nucleation from γ-TuRC was measured as follows. A kymograph was generated for every MT nucleated in the field of view. For most nucleation events, the time of nucleation of the MT was obtained from observing the kymograph and manually recording the initiation time point (see Fig. 1C for examples). For MTs where nucleation occurred before the timelapse movie began or where the initiation was not clearly observed in the kymograph, the shortest length of the MT that was clearly visible in the timelapse was measured and measured average growth speed of MTs was used to estimate the time of nucleation. We verified that this procedure accurately estimates the nucleation time for test case MTs where the nucleation event was visible. The measurement of number of MTs ($N(t)$) nucleated versus time was generated from a manual log containing the nucleation time for all MTs observed in the field of view. To represent the theoretical field-to-field heterogeneity in the number of MTs nucleated, we assumed that binding

of γ-TuRC and subsequent nucleation follows a Poisson distribution with mean n MTs and standard deviation $\sqrt{n}$ MTs. 95% confidence interval in the nucleation measurements, $n \pm 2\sqrt{n}$ is displayed on each nucleation time course.

To calculate the percentage of γ-TuRCs that nucleate a MT, we visualized MT nucleation from Alexa-568 labelled γ-TuRC in the presence of 21μM tubulin and 100nM XMAP215, or with 10.5μM tubulin. We counted the number of labelled γ-TuRC molecules attached in the field of view and counted the number of MTs nucleated specifically from these molecules but excluded spontaneous MT nucleation. For the reaction with 21μM tubulin and 100nM XMAP215, we directly measured that 15% of γ-TuRC molecules nucleated a MT. For the reaction with 10.5μM tubulin, a similar calculation was performed and using measured curves (Fig. 2C), we estimated the percentage of γ-TuRC that will nucleate with 21μM tubulin as 11%.

Power-law analysis of critical nucleus size on γ-TuRC

We consider the following simplified model to determine the number of αβ-tubulin dimers in the rate-limiting, transition state on γ-TuRC i.e. the critical nucleus. We consider a total number of γ-TuRC molecules N_0 available to nucleate MTs at a specific αβ-tubulin concentration C. The total number of MTs nucleated $N(t)$ from a total N_0 γ-TuRCs is a function of time t. If n tubulin dimers assemble cooperatively on γ-TuRC for a successful MT nucleation, the rate of MT nucleation from γ-TuRC molecules available to nucleated at time t, $N_0 - N(t)$ reads,

$$\frac{dN(t)}{dt} = k_{nucleate}(N_0 - N(t))C^n \quad (1)$$

Here we assume that tubulin does not get significantly depleted over time in the course of our reactions as shown by previous calculations[68]. At the start of the reaction $t = 0$, no MTs have

nucleated $N(t=0)=0$, therefore at early times we assume $N_0 - N(t) \approx N_0$ to simplify the calculation of the critical MT nucleus,

$$\left.\frac{dN}{dt}\right|_{t\to 0} = k_{nucleate} N_0 C^n \quad (2)$$

Converting into log scale,

$$ln\left(\left.\frac{dN}{dt}\right|_{t\to 0}\right) = n\, ln(C) + a \quad (3)$$

To obtain the number of αβ-tubulin dimers in the critical nucleus on γ-TuRC, a straight line was fit to the initial, linear region of each nucleation curve $N(t)$ versus t curve for every tubulin concentration C and the rate of nucleation $\left.\frac{dN}{dt}\right|_{t\to 0}$ was obtained from slope of this fit. A straight line was then fit to $ln\left(\left.\frac{dN}{dt}\right|_{t\to 0}\right)$ versus $ln(C)$ for all concentrations, the slope of which provides the size of critical nucleus n. Finally, the measured rate of nucleation depends on the total number of γ-TuRC molecules available. As the total number of γ-TuRC molecules obtained from different days purifications changes, the rate of nucleation from γ-TuRCs at 10.5μM tubulin was set to 1 (normalization factor) to allow pooling of all datasets for γ-TuRC-mediated nucleation.

Spontaneous microtubule nucleation and data analysis

Spontaneous MT assembly was visualized similar to γ-TuRC-mediated nucleation with the following changes. The Pluronic, casein and NeutrAvidin incubations were performed identical to γ-TuRC nucleation assay but instead of attaching γ-TuRCs, sucrose-based buffer (of the same composition as used for γ-TuRC elution) was diluted 5-fold with BRB80, introduced in the flow chamber and incubated for 10 minutes. Washes were performed with 1 vol of BRB80, nucleation mix was added, and imaging was performed as described above. MTs nucleate spontaneously in solution fall down on the coverslip due to depletion forces during the 10 minutes of visualizing the

reaction. The number of MTs nucleated in the field of view were counted manually and plotted in Fig. 3B. 95% confidence interval is displayed assuming a Poisson distribution for theoretical field-to-field heterogeneity as described above.

In the absence of any attached nucleation site, the spontaneously nucleated MTs are usually not visualized from the time of their nucleation and the analysis used for γ-TuRC mediated nucleation was adapted. Integrating the equation (2) above

$$N(t) = k_{nucleate} N_0 C^n t \quad (4)$$

Converting into log scale at time $t = \tau$,

$$ln(N(t = \tau)) = n\, ln(C) + b \quad (5)$$

To obtain the number of αβ-tubulin dimers in the critical nucleus in spontaneous assembly, the number of MTs at a specified time t =7.5 min was measured, a straight line was then fit to $ln(N(t = \tau))$ versus $ln(C)$ for all concentrations, the slope of which provides the size of critical nucleus n. All datasets were pooled and reported.

Preparation, microtubule assembly from blunt microtubule seeds and data analysis

Blunt MTs were prepared with GMPCPP nucleotide in two polymerization cycles as described recently[25]. Briefly, a 50 µl reaction mixture was prepared with 20 µM bovine brain tubulin with 5% Alexa-568 labeled tubulin and 5% biotin-labeled tubulin, 1mM GMPCPP (Jena Bioscience) in BRB80 buffer, incubated on ice for 5 minutes, then incubated on 37°C for 30 minutes to polymerize MTs, and MTs were pelleted by centrifugation at 126,000 xg for 8 minutes at 30°C in TLA100 (Beckman Coulter). Supernatant was discarded, MTs were resuspended in 80% original volume of BRB80, incubated on ice for 20 minutes to depolymerize MTs, fresh GMPCPP was added to final 1mM, incubated on ice for 5 minutes, a second cycle of polymerization was

881 performed by incubating the mixture at 37°C for 30 minutes, and MTs were pelleted again by
882 centrifugation. Supernatant was discarded and MTs were resuspended in 200µl warm BRB80,
883 flash frozen in liquid nitrogen in 5µl aliquots, stored at -80°C and found to be stable for months.
884 To verify that these MT seeds have blunt ends, frozen aliquots were quickly thawed at 37°C,
885 diluted 20-fold with warm BRB80, and incubated at room temperature for 30 minutes to ensure
886 blunt ends as described previously[25]. MTs were pipetted onto CF400-Cu grids (Electron
887 Microscopy Sciences), incubated at room temperature for 60 seconds and then wicked away. 2%
888 uranyl acetate was applied to the grids for 30 seconds, wicked away, and the grids were air-dried
889 for 10 minutes. The grids were imaged using Phillips CM100 TEM microscope at 130000 x
890 magnification and most MT ends were found to be blunt.

891 To assay MT assembly from blunt MT seeds, MT assembly experiments similar to γ-TuRC
892 nucleation assays were performed with the following variation. A lower concentration 0.05 mg/ml
893 NeutrAvidin (A2666, ThermoFisher) was attached, and washes were performed with warm
894 BRB80 prior to attaching MTs. One aliquot of MT seeds was thawed quickly, diluted to 100-fold
895 with warm BRB80, incubated in the chamber for 5 minutes, unattached seeds were washed with 1
896 vol of warm BRB80, and the slide was incubated at room temperature for 30 minutes to ensure
897 blunt MT ends. Wide bore pipette tips were used for handling MT seeds to minimize the shear
898 forces that may result in breakage of MTs. Nucleation mix was prepared as described above and a
899 low αβ-tubulin concentration (1.4-8.7 µM) was used. MT assembly from blunt seeds was observed
900 immediately after incubating the slide on the objective heater. Imaging and analysis were
901 performed as described above for to γ-TuRC nucleation assays. The probability curves $p(t)$ for
902 MT assembly were obtained by normalizing for the total number of seeds observed in the field of
903 view $N(t)/N_0$, which allow for direct comparison across datasets. 95% confidence interval

represents the theoretical variation in the number of MTs assembled from seeds across fields of view as described above. Rate of nucleation $\frac{dp}{dt}\Big|_{t\to 0}$ was obtained as the slope of a straight line fit to the initial region of $p(t)$ versus t curve for every tubulin concentration C. Power-law analysis was performed similar to γ-TuRC nucleation assays described above. However, as assembly from seeds occur near minimal tubulin concentration needed for polymerization of the plus end C_*, the governing equation reads,

$$\frac{dp(t)}{dt} = k_{nucleate}(1 - p(t))C^{n-1}(C - C_*) \quad (6)$$

At the start of the reaction $t = 0$, no MTs have nucleated $p(t = 0) = 0$, therefore at early times we assume $1 - p(t) \approx 1$ to simplify the calculation of the critical MT nucleus. Converting equation (6) in log scale with these simplifications,

$$ln\left(\frac{dp}{dt}\Big|_{t\to 0}\right) = (n - 1)ln(C) + ln(C - C_*) + a \quad (7)$$

Critical tubulin concentration for polymerization C_* was obtained from the x-intercept of the growth speed curve ($C_* = 1.4\mu M$) as described previously. Finally, observing the total number of MT seeds for assembly allows for direct pooling of all datasets for MT assembly from seeds. From fitting a straight line between $ln\left(\frac{dp}{dt}\Big|_{t\to 0}\right)$ versus $ln(C - C_*)$ for all concentrations, we found the slope $n \approx 1$, which satisfies the above equation and provides the size of critical nucleus for MT assembly from seeds $n \approx 1$.

Size exclusion chromatography of γ-tubulin and αβ-tubulin

Size exclusion chromatography of γ-tubulin and αβ-tubulin was performed as follows at 4°C. Purified, human γ-tubulin was diluted to 300nM in γ-TB buffer (defined 50mM K-MES pH6.6, 5mM MgCl2, 1mM EGTA, 10mM thioglycerol, 10μM GDP) with additional 250mM KCl, and

αβ-tubulin individually diluted to 20μM or 70μM with BRB80 buffer. Protein aggregates were pelleted by ultracentrifugation of the proteins individually at 80,000 rpm in TLA 100 (Beckman Coulter) for 15 minutes. γ-tubulin and αβ-tubulin were mixed in 1:1 volume ratio to achieve final concentrations 150nM γ-tubulin to 10μM or 35μM αβ-tubulin and incubated on ice for 10 minutes. 500μl of the mixture was loaded onto Superdex 200 Increase 10/300 column (GE Healthcare). The column was equilibrated with γ-TB buffer containing 90 mM KCl and chromatography was performed in this buffer. For control chromatography runs, equal volume of corresponding buffer was used. Absorbance at 214 nm was recorded. 0.3ml fractions were collected and alternate fractions eluted between 8.5ml and 16.6ml were analyzed via immunoblot against γ-tubulin, αβ-tubulin and StrepII tag on γ-tubulin. Secondary antibody conjugated to 800nm IRDye (LI-COR) was used and imaged with Odyssey CLx imaging station (LI-COR). High molecular weight gel filtration standards (Thyroglobulin, Aldolase and Ovalbumin) were purchased from GE Healthcare (Catalog #28403842) and used to estimate the Stokes' radii of eluted proteins in the same buffer as used for corresponding SEC run[69].

Measurement of affinity between γ-tubulin and αβ-tubulin with single molecule microscopy

γ-TuRC nucleation assay was adapted as follows to measure the interaction affinity between γ-tubulin and αβ-tubulin. The imaging channel was prepared by sequentially with 5% w/v Pluronic F-127 incubation, casein buffer washes, 0.05 mg/ml NeutrAvidin incubation in casein buffer, BRB80 washes as described above. 100-200nM of biotinylated αβ-tubulin or BRB80 buffer was introduced in the flow chamber and incubated for 5 minutes on a cold block, and unbound αβ-tubulin was washed with 50μl of BRB80. During the incubations, binding mix was prepared with 100nM of Alexa-568 or Alexa-488 labelled αβ-tubulin (24-50% labelling percentage) or with

949 100nM of labelled γ-tubulin with identical fluorophore (7% labelling percentage) in 1x assay
950 buffer, ultracentrifuged for 12 minutes in TLA100, oxygen scavengers were added, and reaction
951 mixture was introduced into the flow chamber.

952 Single molecule binding of fluorescent γ-tubulin or αβ-tubulin with biotinylated αβ-tubulin
953 was visualized with TIRF microscopy using the setup described above at 33.5°C. Images were
954 collected at 2-5 fps with EMCCD gain of 300 and exposure time of 200 ms each frame, and data
955 acquisition was started within 60-90 seconds after flowing fluorescent γ-tubulin or αβ-tubulin.
956 Minimal photobleaching was observed for the first 15 seconds of time series acquired, which was
957 used to extract the number by molecules bound by analyzing with the single molecule analysis
958 software ThunderSTORM[70]. Specifically, images were filtered with wavelet B-spline filter (scale
959 2-3 and order 3), molecules localized with 8-connected local maximum approach, threshold
960 selected as the standard deviation of the first wavelet level, and suggested settings for sub-pixel
961 localization by fitting an integrated Gaussian PSF model with maximum likelihood estimation was
962 performed. The number of single molecules identified for each frame were recorded. The results
963 from ThunderSTORM analysis were verified against manually identified molecules with a sample
964 dataset. To obtain how many molecules bind to biotin-αβ-tubulin for every frame, the number of
965 molecules of γ-tubulin or αβ-tubulin bound inspecifically to the coverslip were independently
966 subtracted from the number of molecules bound to biotin-αβ-tubulin, and this value was divided
967 by the known fluorescent labelling percentage. The calculated number of γ-tubulin or αβ-tubulin
968 bound were averaged for the first 14 seconds (28 frames) for each dataset, and their mean and
969 standard deviation was reported.

970 Interaction assays between αβ-tubulin and γ-tubulin were confirmed with biolayer
971 interferometry using Octet RED96e (ForteBio) instrument in an 8-channel plate format. The plate

temperature was held at 33°C and the protein samples were shaken at 400 rpm during the experiment. First, Streptavidin coated biosensors (ForteBio) were rinsed in interaction buffer (50mM K-MES pH 6.6, 100mM KCl, 5mM $MgCl_2$, 1mM EGTA, 0.05% Tween20, 1mM GTP). 100-400 nM biotin-labeled αβ-tubulin, or blank buffer, was bound to Streptavidin sensor until loaded protein results in a wavelength shift (Δλ) of 3 nm. Unbound protein was removed by rinsing the sensor in interaction buffer, and interaction with αβ-tubulin was measured by incubating the sensor containing biotinylated αβ-tubulin with 0-35 μM unlabeled αβ-tubulin or 0-1 μM unlabeled γ-tubulin in interaction buffer for 5 minutes. Δλ (nm) was recorded as a measure of the amount of unlabeled αβ-tubulin that binds to the sensor.

Nucleation of microtubules from purified γ-tubulin

MT assembly experiments from purified γ-tubulin was performed similar to γ-TuRC nucleation assays described above with following variation. No avidin was attached to the coverslips, and varying concentration of γ-tubulin was prepared by diluting purified γ-tubulin in a high salt buffer (50mM K-MES pH 6.6, 500mM KCl, 5mM $MgCl_2$, 1mM EGTA), centrifuging to remove aggregates separately for 12 minutes in TLA100 before adding to the nucleation mix containing 15 μM αβ-tubulin (5% Cy5-labeled) with BSA, glucose oxidase and catalase as described above to a final salt concentration of 44mM KCl. The reaction mixture was introduced into the flow chamber and imaged via TIRF microscopy. A large number of MTs get nucleated immediately in the presence of 250 nM-1000 nM γ-tubulin.

Negative stain electron microscopy of γ-tubulin filaments

Purified γ-tubulin was observed to form higher order oligomers previously using analytical gel filtration[29]. γ-tubulin filaments were prepared by diluting pure γ-tubulin to 1μM to the buffer 50mM K-MES pH 6.6, 5mM $MgCl_2$, 1mM EGTA, 100mM KCl. 5 μl of γ-tubulin mixture was pipetted onto EM grids (Electron Microscopy Sciences, Catalog number: CF400-Cu), which were glow discharged for 25 seconds. 5 μl sample was incubated on the grid at room temperature for 60 seconds and wicked away with filter paper (cat #). Grids were washed with 5 μl of dH_2O 3 times, stained three times with 0.75% Uranyl formate, where the first two incubations were wicked away immediately while the last was incubated for 30 seconds. The grids were air-dried for 10 minutes. Data were collected on a Talos L120C TEM (FEI) equipped with a BM Ceta CCD camera, at a nominal magnification of 74,000x corresponding to a pixel size of 2.03 Å/pixel on the specimen with 1 second integration time, and a defocus range of 1-2 μm underfocus. Micrographs were acquired both in-plane with +0 degree tilt.

Micrographs were converted to mrc file format with IMOD package and imported into RELION-3.0.6[71] where the data analysis was performed. Contrast transfer function (CTF) estimation of 370 micrographs performed using Gctf[72]. Segments along the length of thin filaments were picked manually. Filaments were boxed into helical segments with 50Å rise, and subjected to two rounds of 2D classification and particle selection. 1001 particles were selected and were used to generate an ab-initio 3D model. One round of refinement using 3D auto-refine was performed with all particles, followed by one round of 3D classification. 659 particles from the most populated 3D class were selected and another round of refinement was performed to generate a final map with the solvent mask. Analysis was performed in UCSF Chimera[73]. Longitudinal arrangement of αβ-tubulins (pink filament, Fig. 4-supplement 2E) was generated by isolating one protofilament from PDB: 6DPU[38] and elongating the protofilament with the super-position

function in Coot. Lateral arrangement of γ-tubulin array (blue filament, Fig. 4-supplement 2E) was generated from the crystal contacts observed in the published P21 crystal array (PDB: 1Z5W[40]), as described previously[39]. An alternate γ-tubulin arrangement was also generated by isolating the other possible filament from this P21 symmetry group, where neighboring γ-tubulins neither arrange linearly nor show lateral contacts (green filament, Fig. 4-supplement 2E). Simultaneous docking of 4 copies each of longitudinal αβ-tubulin array, lateral γ-tubulin array, or alternate arrangement of γ-tubulin array, was performed by fitting each copy at 15Å resolution in UCSF Chimera using the fitmap function. Lateral γ-tubulin arrays, but not other filament arrangements, display good fit where the γ-tubulin spacing closely matches that of the reconstructed filaments.

Monte Carlo simulations of microtubule nucleation by γ-TuRC

Simulation procedure

Kinetic Monte Carlo simulations for MT nucleation and assembly by γ-TuRC were coded and run in MATLAB and were based on a previous stochastic model for the plus-end dynamics of a MT[41]. A type-B MT lattice geometry with 13-protofilaments and a pitch of 3 tubulins at the seam was assumed, and a similar γ-TuRC geometry was encoded. On the blunt plus-end geometry, αβ-tubulin dimers in the MT lattice may have no neighbors, one or half a neighbor at the seam. Once the MT growth occurs into a tapered one, αβ-tubulin dimers can also have one or two neighbors.

New αβ-tubulin dimers arrive with a constant on rate, k_{on} ($M^{-1}s^{-1}$) on each protofilament. This on rate is equal for each protofilament on the plus-end or on γ-TuRC and remains constant during the simulation. An input concentration of αβ-tubulin dimers was assumed to be constant and not be depleted as shown by previous calculations[68]. Therefore, the net on-rate at each time step is, $k_{on}C$ (s^{-1}), where C is the concentration of αβ-tubulin dimers. The interactions between

αβ-tubulins was assumed to occur with longitudinal and lateral bond energies, $\Delta G_{Long,\alpha\beta-\alpha\beta}$ and $\Delta G_{Lat,\alpha\beta-\alpha\beta}$, respectively. All αβ-tubulin dimers recruited to the MT lattice or γ-TuRC have a longitudinal bond, and the lateral bond energy depends on the arrangement of neighboring αβ-tubulin dimers. The longitudinal bond energy between γ-/αβ-tubulin on γ-TuRC is $\Delta G_{Long,\gamma-\alpha\beta}$. As a result, the dissociation rate (off-rate) of individual tubulin dimers from the lattice differs and is a function of total bond energy ΔG_{tot}. ΔG_{tot} is a sum of the longitudinal bond energy, $\Delta G_{Long,\alpha\beta-\alpha\beta}$ or $\Delta G_{Long,\gamma-\alpha\beta}$, plus the total lateral bond energy from all the neighbors, $m \times \Delta G_{Lat,\alpha\beta-\alpha\beta}$. Based on previous works, we also posit that when a tubulin dimer dissociates, all dimers above it in the protofilament dissociate as well. The off-rate of each dimer was then calculated from the following equation as derived previously[41],

$$lnK = ln\left(\frac{k_{on}}{k_{off}\,(s^{-1})}\right) = -\frac{\Delta G_{tot}}{k_B T} \quad (8)$$

An open conformation of native γ-TuRC was assumed as observed in recent cryo-EM structures[13–15]. The αβ-tubulins assembled on neighboring sites do not form lateral interactions in the open conformation. A possible transition to a closed γ-TuRC state was allowed with a thermodynamic penalty of $\Delta G_{\gamma TuRC-conf}$. However, if n lateral bonds form upon this transition from αβ-tubulins assembled on neighboring sites, that net energy for an open-to-closed transition is $\Delta G_{close} = \Delta G_{\gamma TuRC-conf} - n\Delta G_{Lat,\alpha\beta-\alpha\beta}$. At each time step in the simulation, the rate of this transition is calculated as, $k_{\gamma TuRC-conf} \times \exp\left(\frac{-\Delta G_{close}}{k_B T}\right)$, where $k_{\gamma TuRC-conf}\,(s^{-1})$ is the pre-factor of the Arrhenius equation. Hydrolysis of incorporated tubulin dimers was ignored because few catastrophe events were observed in our experiments.

To execute the stochastic simulations, we formulate a list of possible events at every time step, including association of a αβ-tubulin dimer, dissociation of a αβ-tubulin dimer, or transition

of γ-TuRC to closed state. The forward rate of each event is calculated as described above. A uniform random number (R_i) from 0 to 1 is generated for each possible event in the list and a single realization of the exponentially distributed time is obtained for each event,

$$t_i = \frac{-\ln(R_i)}{k_i\,(s^{-1})} \quad (9)$$

The event with the shortest execution time is implemented and time elapsed during the simulation is advanced by t_i seconds. Each simulation was run with a maximum defined time, usually between 100-500 seconds, or were stopped once the MT grew a total of 2-5μm in length. The MATLAB code for simulations is provided in the Supplementary Materials.

Parameter estimation

MT growth parameters were determined by fitting to experimental growth speed curves. Briefly, 20 simulations were performed for each concentration from 2-20μM tubulin for 100 seconds each. MT length versus time was plotted. Growth speed was obtained from the slope of a linear curve fit of the polymerizing stretch of the length versus time plot. Parameter values of $k_{on} = 1.3 \times 10^6\ (\mu M^{-1}s^{-1}), \Delta G_{Long,\alpha\beta-\alpha\beta} = -7.2k_BT, \Delta G_{Lat,\alpha\beta-\alpha\beta} = -6.5k_BT$ resulted in the best fit for all tubulin concentrations. These parameter values are similar to those obtained in previous reports[31,41]. With these polymerization parameters fixed, we varied the remaining parameters. $\Delta G_{Long,\gamma-\alpha\beta}$ was varied from $(0.7 - 1.3) \times \Delta G_{Long,\alpha\beta-\alpha\beta}$. $\Delta G_{\gamma TuRC-conf}$ was varied from $+(0 - 30)k_BT$ and $k_{\gamma TuRC-conf}$ from $(1 - 0.001)\ s^{-1}$. For each parameter set, we performed 200-500 simulations each at specific tubulin concentrations between 2-50μM. For each simulation, the time of γ-TuRC ring closure was recorded as the nucleation time as it represents the transition from zero MT length to a continuously growing MT. For the simulation where no MT nucleation occurred, a nucleation time of infinity was recorded. Cumulative probability distribution of

nucleation ($p(t)$) versus time was generated from the log of nucleation times for each tubulin concentration. Rate of nucleation $\left.\frac{dp}{dt}\right|_{t\to 0}$ was obtained by a linear fit from the initial part of each nucleation fit, as described above. The slope of a straight line was fit to $ln\left(\left.\frac{dp}{dt}\right|_{t\to 0}\right)$ versus $ln(C)$, as outlined in equations (2-3) above, provide the size of critical nucleus n. The nucleation curves and power-law analysis was compared with experimental data for γ-TuRC-mediated nucleation. The best agreement was found with $\Delta G_{Long,\gamma-\alpha\beta} = 1.1 \times \Delta G_{Long,\alpha\beta-\alpha\beta}$, as supported by our biochemical measurements, $\Delta G_{\gamma TuRC-conf} = 10 k_B T$ and $k_{\gamma TuRC-conf}$=0.01 s^{-1}.

To analyze the arrangement of αβ-tubulins in the transition state, the state of γ-TuRC with αβ-tubulin dimers was recorded at the time of γ-TuRC ring closure for 2119 simulations. 3D-dimensional probability distribution of total number of αβ-tubulin dimers and number of lateral αβ-tubulin bonds was generated. The arrangement of αβ-tubulin dimers in the most frequently occurring transition states were displayed with schematics.

To capture the dynamics of MT assembly from blunt seeds, we simulated nucleation assuming a closed γ-TuRC geometry as follows. Lateral bonds between αβ-tubulins assembled on the neighboring sites on γ-TuRC were allowed and $\Delta G_{Long,\gamma-\alpha\beta}$ was set equal to $\Delta G_{Long,\alpha\beta-\alpha\beta}$. Simulations were performed as described above with the following change. The time when the MT in each simulation grew to 50nm length was recorded to generate the probability distribution. Nucleation curves and power-law analysis was compared with experimental data for seed-mediated MT assembly.

Measuring the effect of microtubule associated proteins on γ-TuRC-mediated nucleation

Effect of microtubule associated proteins (MAPs) was measured on γ-TuRC's nucleation activity. γ-TuRC was attached on the coverslips using the setup described above and a control experiment

was performed with identical reaction conditions for each protein tested. Because CDK5RAP2's γ-TuNA motif and NME7 bind γ-TuRC, to test their activity γ-TuRC was additionally incubated 6μM γ-TuNA motif or 6μM NME7 to γ-TuRC for 5 minutes prior to attachment to coverslips to maximize their likelihood of binding and the control γ-TuRC reaction was treated identically with the storage buffer for each protein. Nucleation mix was then prepared containing 10.5 μM αβ-tubulin concentration (5% Cy5-labeled tubulin) as specified along with 1mg/ml BSA and oxygen scavengers, and either buffer (control), 10nM GFP-TPX2, 3μM γ-TuNA motif from CDK5RAP2, 6μM NME7, 5μM Stathmin or 10nM MCAK was added. To test NME7 or MCAK's effect, the assay buffer additionally contained 1mM ATP. The reaction mixture containing tubulin and MAP at specified concentration was introduced into the flow chamber containing γ-TuRC, and MT nucleation was visualized by imaging the Cy5-fluorescent channel at 0.5-1 frames per second. For TPX2, fluorescence intensity of the protein was simultaneously acquired.

The number of MTs nucleated over time was measured as described above and the effect of protein on γ-TuRC's nucleation activity was assessed by comparing nucleation curves with and without the MAP. In order to normalize for the total number of γ-TuRC molecules obtained from different purifications and enable pooling results from all datasets, the number of MTs nucleated at a specified time point, mentioned in each figure legend, was set to 1 for γ-TuRC only (no MAP) control reactions. As before the shaded region represents 95% confidence interval ($n \pm 2\sqrt{n}$) in the number of MTs, n assuming a Poisson distribution that determines binding and subsequent nucleation from γ-TuRCs and was calculated and displayed on each nucleation time-course.

Cooperative microtubule nucleation assay with purified XMAP215 and γ-TuRC

A similar set of experiments as above to characterize the effect of MAPs was performed to study the effect of XMAP215 on γ-TuRC-mediated nucleation with the single molecule assays with the following differences. 20nM of XMAP215-GFP-7xHis was added to nucleation mix prepared with 3.5-7 μM αβ-tubulin concentration (5% Cy5-label) in XMAP assay buffer (80mM K-PIPES, 1mM $MgCl_2$, 1mM EGTA, 30mM KCl, 0.075% w/v methylcellulose 4000 cp, 1% w/v D-(+)-glucose, 0.007% w/v Brij-35, 5mM BME, 1mM GTP). MTs nucleated from attached γ-TuRC with and without XMAP215 were measured to assess the efficiency of nucleation induced by XMAP215. To assess if N- or C-terminal domains of XMAP215 increases nucleation efficiency, wild-type XMAP215 was replaced with a C-terminal construct of XMAP215 (TOG5-Cterminus-GFP) or an N-terminal construct (TOGs1-4-GFP) in the described experiment.

To measure the kinetics of cooperative nucleation XMAP215 and γ-TuRC, a constant density of γ-TuRC was attached as described above and nucleation mix nucleation mix was prepared with a range of αβ-tubulin concentration between 1.6-7 μM (5% Cy5-label) with 20-25nM of XMAP215-GFP-7xHis or XMAP215-TEV-GFP-7xHis-StrepII in XMAP assay buffer, introduced into reaction chamber and MT nucleation was imaged immediately by capturing dual color images of XMAP215 and tubulin intensity at 0.5 frames per second.

Data analysis was performed as above for γ-TuRC mediated nucleation, theoretical field-to-field heterogeneity in the number of MTs nucleated was represented with a Poisson distribution as before and 95% confidence interval. Critical tubulin nucleus for cooperative nucleation from XMAP215 and γ-TuRC was obtained as described for γ-TuRC alone (equations (1-3)). A straight line was fit to log rate of nucleation $ln\left(\frac{dN}{dt}\Big|_{t\to 0}\right)$ versus log tubulin concentration $ln(C)$ and its slope provides the size of critical nucleus n. Finally, to normalize for the total number of γ-TuRC

molecules obtained from different purifications, the rate of cooperative nucleation from XMAP215 and γ-TuRC at 3.5μM tubulin was set to 1. All datasets were pooled and reported.

Triple-color imaging of XMAP215, γ-TuRC and microtubules

For triple-color fluorescence assays, Alexa-568 and biotin-conjugated γ-TuRC was first attached to coverslips as described above with the following variation: 0.05 mg/ml of NeutrAvidin was used for attaching γ-TuRC. Nucleation mix was prepared with 7μM αβ-tubulin (5% Cy5-label), 10nM Alexa-488 XMAP215-SNAP or XMAP215-GFP with BSA and oxygen scavengers in XMAP assay buffer (80mM K-PIPES, 1mM $MgCl_2$, 1mM EGTA, 30mM KCl, 0.075% w/v methylcellulose 4000 cp, 1% w/v D-(+)-glucose, 0.007% w/v Brij-35, 5mM BME, 1mM GTP) and introduced into the reaction chamber containing attached γ-TuRC. Three-color imaging per frame was performed with sequential 488, 568 and 647 nm excitation and images were acquired with EMCCD camera at 0.3 frames per second.

Figure legends

Figure 1. Single molecule microscopy of microtubule nucleation from γ-TuRC.

(A) Schematic for microtubule nucleation from γ-TuRC. Biochemical features of γ-TuRC including the γ-/αβ-tubulin interaction affinity and conformation of γ-TuRC determine to MT nucleation activity and transition state. (B) Purified, biotinylated γ-TuRC molecules were attached, incubated with αβ-tubulin and time-lapse of MT nucleation after is shown. MTs already nucleated in the first frame are marked with yellow arrow, while new MT nucleation events between the first and last frame with blue arrows. (C) Three representative kymographs of (left) unlabeled γ-TuRC nucleating MTs colored in grayscale, or (right) fluorescent γ-TuRC, pseudo-colored in green, nucleating MTs, pseudo-colored in red. Arrows point to nucleation sites. The experiments with unlabeled γ-TuRC were repeated more than ten times with independent γ-TuRC preparations, while those fluorescent γ-TuRC repeated were repeated six times with three independent γ-TuRC preparations. See Figure 1-figure supplement 1 and Videos 1-2.

Figure 2. Molecular composition of transition state in γ-TuRC-mediated nucleation.

(A) Titrating tubulin concentration with constant the density of γ-TuRC. MT nucleation from γ-TuRC begins at 7μM tubulin. (B) MT plus-end growth speed increases linearly with tubulin concentration. Individual data points are plotted, and linear fit (red line) with shaded mean±2std (95% confidence interval) is displayed. Critical concentration for polymerization as $C^* = 1.4$ μM. Inset: Number of MTs nucleated by γ-TuRCs within 120 seconds varies non-linearly with tubulin concentration. (C) Number of MTs nucleated ($N(t)$) over time (t) is plotted for varying tubulin concentration to obtain rate of nucleation as the slope of the initial part of the curves. Shaded

regions represent 95% confidence interval $(n \pm 2\sqrt{n})$ in the number of nucleated MTs (n) assuming a Poisson distribution as described in Methods. (D) Number of tubulin dimers (n) in the critical nucleus on γ-TuRC was obtained as 3.9±0.5 from the equation $\frac{dN}{dt}\Big|_{t\to 0} = kC_{tub}{}^{n}$ displayed on a log-log axis as detailed in Methods. The rate of nucleation at 10.5μM was set to 1 to normalize differences in γ-TuRC concentration from individual experiments. The experiments and analyses in (A-D) were repeated identically three times with independent γ-TuRC preparations. MT nucleation data, prior to normalization, from one representative dataset is displayed in (B-C). Analyses from all repeats was pooled and normalized as described above, and data points from 15 nucleation-time curves are plotted in (D). See Video 3.

Figure 3. Comparison of γ-TuRC-mediated, spontaneous and seed-templated nucleation.

(A) Spontaneous MT nucleation (schematized) was measured with increasing tubulin concentration and high concentrations. 14μM tubulin is required. (B) Number of MTs ($N(t=\tau)$) nucleated spontaneously were plotted against tubulin concentration. Power-law curve was fit as $N(t=\tau) = kC^n$ on a log-log axis, and linear scale in the inset. Tubulin cooperativity (exponent) of n = 8.1±0.9 was obtained as detailed in Methods. Experiments and analyses in (A-B) were repeated thrice independently, all data were pooled and data points from 11 nucleation curves are plotted in (B). In the inset, data is represented in linear plot, where shaded regions represent 95% confidence interval $(n \pm 2\sqrt{n})$ in the number of nucleated MTs (n) assuming a Poisson distribution as described in Methods. Scale bars, 10μm. (C) Schematic and an example micrograph of blunt, stabilized MT seeds is shown and MT assembly from them was observed (bottom) with varying tubulin concentration. (D) Cumulative probability of MT assembly from seeds ($p(t)$) over time (t) is plotted and rate of nucleation was obtained as the slope from initial part of the curves.

Shaded regions represent 95% confidence interval ($n \pm 2\sqrt{n}$) in the number of MTs assembled (n) from seeds as described in Methods. (E) As described in Methods, the measurements fit well to equation $\frac{dp}{dt}\Big|_{t\to 0} = k(C - C^*)^n$ displayed on a log-log plot. n = 1±0.3 was obtained showing nearly non-cooperative assembly of tubulin dimers. The experiments and analyses in (C-E) were repeated three times independently. MT nucleation data, prior to normalization, from one representative dataset is displayed in (C-D). Analyses from all experiments was pooled, and data points from a total of 11 nucleation-time curves are reported in (E). See Figure 3-figure supplement 1 and Videos 4-5.

Figure 4. γ-tubulin binds to αβ-tubulin with a high affinity.

(A) Size-exclusion chromatography was performed with 150nM of γ-tubulin alone (i) and with 35μM and 10μM αβ-tubulin in (ii) and (iii) respectively. Gel filtration fractions were analyzed via SDS–PAGE followed by immunoblot with γ-tubulin and αβ-tubulin antibodies. A shift in the γ-tubulin elution to fraction H was observed with both 35μM and 10μM αβ-tubulin, denoting complex formation with αβ-tubulin. See Fig. 4-figure supplement 1A. Stokes' radii of reference proteins: thyroglobulin (8.6 nm), aldolase (4.6 nm) and ovalbumin (2.8 nm), are marked at their elution peak. Size exclusion runs were repeated three times, with the exception of 10μM αβ-tubulin run that was performed twice. (B) Single molecule microscopy was performed with γ-tubulin and αβ-tubulin. Control buffer (left panels, (i) and (ii)) or biotinylated αβ-tubulin (right panels, (i) and (ii)) was attached to coverslips, incubated with fluorescent αβ-tubulin (i) or γ-tubulin (ii) molecules, set as 0 seconds, and their binding at 60-90 seconds. (C) Number of bound molecules were analyzed for the first 15 seconds of observation described in Methods. Experiments and analyses in (B-C) were repeated identically two times, pooled and reported. n =56 data points each

were displayed as mean ± std in the bar graph in (C). Further confirmed with a third supporting experimental set where the observation began later at 180 seconds and was therefore, not pooled. See also Figure 4-figure supplements 1-2.

Figure 5. Monte Carlo simulations of microtubule nucleation from γ-TuRC.

(A) Kinetic Monte Carlo simulations of MT nucleation were performed. Helical MT lattice was simulated with 13 protofilaments and a pitch of 3 tubulin monomers across the seam. Native γ-TuRC was simulated in an open conformation and was allowed transition into a closed conformation with a thermodynamic penalty of $\Delta G_{\gamma TuRC-conf}$. αβ-tubulin dimers form longitudinal bonds with energies, $\Delta G_{Long,\gamma-\alpha\beta}$ and $\Delta G_{Long,\alpha\beta-\alpha\beta}$ to γ-tubulin and other αβ-tubulins, respectively, and lateral bond with energy, $\Delta G_{Lat,\alpha\beta-\alpha\beta}$ with neighboring αβ-tubulin dimers. (B) MT length (μm) versus time (seconds) traces of two independent simulations are presented (bottom). MT nucleation occurs are variable time points for each model realization. Zoomed-in insets of the first simulation show the length of the tallest protofilament (nm) and total number of αβ-tubulin dimers assembled in the first 200 msec and 5 sec near the transition state of the simulation. (C) Simulations were performed with $k_{on} = 1.3 \times 10^6\ (M^{-1}s^{-1}pf^{-1})$, $\Delta G_{Long,\alpha\beta-\alpha\beta} = -7.2k_BT$, $\Delta G_{Lat,\alpha\beta-\alpha\beta} = -6.5k_BT$, $\Delta G_{Long,\gamma-\alpha\beta} = 1.1\Delta G_{Long,\alpha\beta-\alpha\beta}$, $k_{\gamma TuRC-conf} = 0.01s^{-1}$. $\Delta G_{\gamma TuRC-conf}$ was varied from $+(0-30)k_BT$. Tubulin concentration was varied from 2.5-50μM. 200 simulations were performed for a given tubulin concentration at every parameter set, except for $\Delta G_{\gamma TuRC-conf} = 10k_BT$ where 500 simulations were performed. From probability of MT nucleation ($p(t)$) versus time (t) curves, the initial rate of nucleation $\left.\frac{dp}{dt}\right|_{t\to 0}$ was measured and plotted against concentration on a log-log axis as detailed in Methods. (D) With the parameters defined above and $\Delta G_{\gamma TuRC-conf} = 10k_BT$, the transition state at the time of γ-

TuRC's conformational change was recorded for *n*=2119 simulations. Normalized histogram of total number of αβ-tubulin dimers is plotted (left). 3-dimensional probability distribution of total number of αβ-tubulin dimers (x) and number of lateral αβ-tubulin interactions (y) is plotted (right). The most populated transition states are denoted with coordinates (x,y) and schematized. See also Figure 5-figure supplements 1-2.

Figure 6. Regulation of γ-TuRC-mediated nucleation by putative activation factors.

(A) A constant density of γ-TuRC molecules were attached without (left) and with (right) 6μM CDK5RAP2's γ-TuNA motif and 10.5μM tubulin ± 3μM additional γ-TuNA was added. Scale bar, 10μm. (B) MTs nucleated from γ-TuRC molecules were analyzed and 3-6μM CDK5RAP2's γ-TuNA motif (left) or 1-6μM NME7 (right). Experiments and analyses in (A-B) were individually repeated twice on different days of experimentation with independent or same γ-TuRC preparations. Number of MTs nucleated in control reactions at 200 seconds for γ-TuNA, and at 150 seconds for NME7 was set to 1 to account for variable γ-TuRC concentration across purifications, all data was pooled and reported. Individual datasets with ±γ-TuNA and ±NME7 is represented with solid or dashed curves. Shaded regions represent 95% confidence interval ($n \pm 2\sqrt{n}$) from each dataset in the number of nucleated MTs (n) assuming a Poisson distribution as described in Methods. (C-D) A constant density of γ-TuRC molecules were attached and 10.5μM tubulin ± 10-20nM GFP-TPX2 was added. Experiments and analyses were repeated thrice with independent γ-TuRC preparations. To account for the variable γ-TuRC concentration across purifications, the number of MTs nucleated in control reactions at 150 seconds was set to 1. All data was pooled and reported. Individual dataset with ±TPX2 is represented with solid, dashed or dotted curves. Shaded regions represent 95% confidence interval ($n \pm 2\sqrt{n}$) from each dataset in

the number of nucleated MTs (n) assuming a Poisson distribution as described in Methods. See Figure 6-figure supplement 1 and Video 6.

Figure 7. Role of XMAP215 and microtubule-associated proteins in microtubule nucleation with γ-TuRC.

(A) γ-TuRCs were attached and 7μM tubulin (pseudo-colored in red) ± 20nM XMAP215-GFP (pseudo-colored in green) was added. Scale bar, 10μm. Experiments and analyses in (A-B) were repeated thrice with independent γ-TuRC preparations. (B) Number of MTs nucleated ($N(t)$) over time (t) was measured and control reactions at 120 seconds was set to 1 to account for variable γ-TuRC concentration across purifications, all data was pooled and reported. Individual datasets with ±XMAP215 is represented with solid or dashed curves. Shaded regions represent 95% confidence interval ($n \pm 2\sqrt{n}$) from each dataset in the number of nucleated MTs (n) assuming a Poisson distribution as described in Methods. See also See Figure 7-figure supplement 1A-B. (C) Sequence of events during cooperative MT nucleation by γ-TuRC and XMAP215 was visualized using labeled γ-TuRC (blue), XMAP215 (red) and tubulin (green) represented in a time sequence and kymograph. γ-TuRC and XMAP215 form a complex prior to MT nucleation. XMAP215 molecules reside on γ-TuRC for before MT nucleation. The experiment was repeated a total of 8 times with two independent γ-TuRC preparations and independent XMAP215 purifications. Scale bar, 5μm. (D-E) Number of MTs nucleated ($N(t)$) over time (t) was measured after titrating tubulin with constant γ-TuRC and XMAP215 concentration. XMAP215/γ-TuRC molecules nucleate MTs from 1.6 μM tubulin. Shaded regions represent 95% confidence interval ($n \pm 2\sqrt{n}$) in the number of nucleated MTs (n) assuming a Poisson distribution as described in Methods. (E) Number of tubulin dimers (n) in the critical nucleus on cooperative nucleation by γ-TuRC/XMAP215 was

obtained as 3.3±0.8 from the equation $\frac{dN}{dt}\Big|_{t\to 0} = kC_{tub}{}^{n}$ displayed on a log-log axis as detailed in Methods. The rate of nucleation at 3.5μM was set to 1 to normalize differences in γ-TuRC concentration from individual experiments. Experiment and analyses in (D-E) was repeated thrice over the entire concentration range with independent γ-TuRC preparations, and fewer concentration points were repeated another two times. All five datasets were pooled and data points from a total of 18 nucleation-time curves are reported in (E). Simulations were adapted to understand how XMAP215 changes the thermodynamics of γ-TuRC-mediated nucleation. Parameter values used: $k_{on} = 1.3 \times 10^{6}\ (M^{-1}s^{-1}pf^{-1})$, $\Delta G_{Long,\alpha\beta-\alpha\beta} = -8.64k_BT$, $\Delta G_{Lat,\alpha\beta-\alpha\beta} = -6.2k_BT$, $\Delta G_{Long,\gamma-\alpha\beta} = -9.5k_BT$, $k_{\gamma TuRC-conf} = 0.01s^{-1}$and $\Delta G_{\gamma TuRC-conf} = 10k_BT$. Compared to simulations for γ-TuRC alone (Figure S6A), either $\Delta G_{Long,\alpha\beta-\alpha\beta}$ was increased 1.2-fold, as proposed previously[41], or both $\Delta G_{Long,\alpha\beta-\alpha\beta}$ and $\Delta G_{Long,\alpha\beta-\alpha\beta}$ were increased 1.2-fold. 200 simulations each were performed for a range of tubulin concentration 1.6-7μM. Probability of MT nucleation ($p(t)$) versus time (t) is displayed in (D). The initial rate of nucleation $\frac{dp}{dt}\Big|_{t\to 0}$ was measured at each tubulin concentration and plotted against concentration on a log-log axis in (E). Linear curve was fit for n=5 simulated data points, and critical nucleus of 3.8 ± 0.3 αβ-tubulins. Increasing all longitudinal bond energies reproduces the effect of XMAP215 on γ-TuRC-mediated nucleation. (F) Number of MTs nucleated was measured to assess the effect of inhibitory MAPs MCAK or Stathmin on γ-TuRC-mediated nucleation. 10.5μM tubulin ± 10nM MCAK, or 7-10.5μM tubulin ± 2-5μM Stathmin was added to attached γ-TuRC- molecules, and MCAK and Stathmin were both found to inhibit γ-TuRC-mediated nucleation. Experiments and analyses for both MAPs were repeated thrice individually with independent γ-TuRC preparations. Number of MTs nucleated in control reactions at 200 seconds

was set to 1 to account for variable γ-TuRC concentration across purifications, all data was pooled and reported. Individual dataset with ± MCAK are reported with solid, dashed or dotted curves. For Stathmin, two datasets for 10.5μM tubulin ± 5μM Stathmin are reported with solid and dashed lines, and one dataset for 7μM tubulin ± 2μM Stathmin in dotted line. Shaded regions represent 95% confidence interval ($n \pm 2\sqrt{n}$) from each dataset in the number of nucleated MTs (n) assuming a Poisson distribution as described in Methods. See Figure 7-figure supplements 1-2 and Videos 7-9.

Supplementary Figure legends

Figure 1-figure supplement 1. Controls for γ-TuRC-mediated microtubule nucleation.

(A) Protein gel of purified γ-TuRC was stained with SYPRO Ruby stain (left). Biotinylated sites on γ-TuRC was visualized with alkaline phosphatase conjugated to avidin (middle), and Alexa-568 labelled subunits of γ-TuRC after additional fluorescent conjugation were visualized on an SDS-PAGE with Typhoon 9500 fluorescence imager (right). Major, known γ-TuRC components were detected in the purified protein and GCP2/3 are heavily biotinylated or Alexa-568 labelled during purification. The experiments were repeated thrice with independent γ-TuRC preparations, with the exception of Alexa-568 scan that was repeated twice. (B) Purified and biotinylated γ-TuRC was stained with uranyl acetate and visualized with transmission electron microscopy. Scale bar, 100nm. The experiments were repeated over ten times with independent γ-TuRC preparations. (C) Fluorescently-labelled and biotinylated γ-TuRC molecules (pseudo-colored as green) were attached, incubated with 10.5μM αβ-tubulin (pseudo-colored as red) and time-lapse of MT nucleation after is shown. γ-TuRCs denoted with yellow arrows have nucleated a MTs before 180 seconds, while those labelled with gray arrows nucleated MTs between 180 and 330 seconds visualized in the time-lapse. Scale bar, 10μm. See Video 2. The experiment was repeated six times with three independent γ-TuRC preparations. (D) MTs were first nucleated from γ-TuRC with Alexa 568-labeled tubulin (pseudo-colored in cyan), followed by introduction of Cy5-labeled tubulin (pseudo-colored in magenta). New tubulin incorporates only on the freely growing, plus-end but not at the nucleated minus-end. Scale bar, 10μm. The experiment was performed three times with two independent γ-TuRC preparations. See also Figures 1-2 and Videos 1-2.

Figure 3-figure supplement 1. Controls for spontaneous and blunt seed-mediated microtubule nucleation.

(A) Representative kymographs of spontaneously nucleated MT is displayed, demonstrating that MTs grow from both the minus-end (dotted line) and the plus-end (solid line) and can be distinguished from γ-TuRC-mediated nucleation. Scale bar, 10μm. Tens of kymographs were generated from at least three independent experiments. (B) Comparison of γ-TuRC-mediated with spontaneous MT nucleation and reactions where γ-TuRC was not attached. MTs were nucleated by attaching purified γ-TuRC (left), adding control buffer to allow for spontaneous MT nucleation (middle) or leaving avidin out to test the level of nucleation by non-specifically attached γ-TuRCs (right). Robust MT nucleation only occurs with γ-TuRC attached to coverslips and not in control reactions. Scale bar, 10μm. (C) MTs nucleation from γ-TuRCs or spontaneously were compared directly at 10.5μM tubulin concentrations. Shaded regions represent 95% confidence interval($n \pm 2\sqrt{n}$) in the number of nucleated MTs (n) assuming a Poisson distribution as described in Methods. γ-TuRC nucleates significantly higher number of MTs than spontaneous assembly. The experimental set and analyses in (B-C) were repeated identically two times with independent γ-TuRC preparations. (D) MTs were assembled from blunt seeds. Tubulin concentration was titrated, and growth speed of MT plus-ends was measured from kymographs (blue circles). Critical concentration (C^* = 1.4 μM) was determined from the linear fit (blue line) with shaded 95% confidence intervals. The experiment and analyses in were repeated thrice with independent seed preparations. The growth speed of MTs assembled from seeds was overlaid with those nucleated from γ-TuRC (Fig. 2B, red circles and line) for comparison. See also Videos 3-5 and Figures 2-3.

Figure 4-figure supplement 1. Purified γ-tubulin binds αβ-tubulin with high affinity *in vitro*.

(A) Size-exclusion chromatography was performed with 35μM and 10μM αβ-tubulin alone in (i) and (ii) respectively. Gel filtration fractions were analyzed via SDS–PAGE followed by immunoblot with αβ-tubulin antibodies. At high concentration (35μM), αβ/αβ-tubulin self-interaction occurs, and oligomeric species elutes in fractions B-C, as seen via the immunoblot and absorbance reading. Oligomeric species is not observed at 10μM αβ-tubulin. Stokes' radii of reference proteins: thyroglobulin (8.6 nm), aldolase (4.6 nm) and ovalbumin (2.8 nm), are marked at their elution peak. Size exclusion runs was repeated three times for 35μM αβ-tubulin and twice for 10μM αβ-tubulin. (B) Molecular interaction between γ/αβ-tubulin was verified with bio-layer interferometry. Buffer ((i) and (ii), left curves) or biotin-tagged αβ-tubulin ((i) and (ii), right curves) was loaded on the probe as bait. Untagged αβ-tubulin (i) at 0-35μM or γ-tubulin (ii) at 0-1μM were used as prey. Wavelength shift, $\Delta\lambda$ (nm) was recorded to estimate the mass of bound protein on the probe. More than 2μM of αβ-tubulin was needed to observe significant binding to biotin-αβ-tubulin. While γ-tubulin non-specifically associates with the probe to a low extent, significant association with biotin-αβ-tubulin over this non-specific binding was observed at significantly lower concentrations. (300nM). The experiments in (i) and (ii) were repeated two times independently. See also Figure 4.

Figure 4-figure supplement 2. Purified γ-tubulin nucleates microtubules and assembles laterally into filaments.

(A) MTs nucleate from high concentration of purified γ-tubulin efficiently and (B) minus-ends of γ-tubulin-nucleated MTs remain capped while the plus-ends polymerize. The experiments were repeated twice for all concentration points, with one additional supporting experimental set with fewer γ-tubulin concentrations. (C) γ-tubulin self-assembles into filaments of variable widths at

high concentration (1-2μM) and physiological salt (100mM KCl) as observed with negative-stain, transmission electron microscopy. Scale bar, 100nm. (D) 3D reconstructions of negatively stained γ-tubulin filaments with thin width shows 4 linearly arrays of interacting γ-tubulins. Repeat distance of approximately 54Å was observed between each γ-tubulin within a linear array. (E) Longitudinal arrangement of αβ-tubulins (pink filament), generated by isolating one protofilament from PDB: 6DPU[37,38], docked into map (see Methods). Repeat distance between longitudinally-interacting αβ-tubulins (40Å) does not match the map spacing (54Å). Lateral arrangement of γ-tubulin array (blue filament) was generated from the crystal contacts observed in the crystal lattice of PDB: 1Z5W[39,40]. An alternate γ-tubulin arrangement was also generated (green filament) was isolated from the other possible filament in this P21 crystal lattice of PDB: 1Z5W. In this arrangement, neither do neighboring γ-tubulins arrange into straight filaments nor do they show lateral contacts (green filament). Both filaments were docked into the one position in the map. Laterally-associated γ-tubulin array (blue filament) display a good fit where the γ-tubulin spacing closely matches that of the reconstructed filament. In the arrangement displayed in the green filament, not only are the alternate γ-tubulins farther apart (61Å) and do not make a direct contact, the alternate γ-tubulins also place off-axis and do not form a linear array. This arrangement does not recapitulate the linear γ-tubulin arrangement where all γ-tubulins are 54Å apart, as observed in the map. Thus, our filaments are composed of laterally-associated, linear γ-tubulin arrays.

Figure 5-figure supplement 1. Parameter variation in Monte Carlo simulations of γ-TuRC-mediated nucleation.

(A) MT plus-end assembly was simulated. Parameter values used: $k_{on} = 1.3 \times 10^6\ (M^{-1}s^{-1}pf^{-1})$, $\Delta G_{Long,\alpha\beta-\alpha\beta} = -7.2k_BT$, $\Delta G_{Lat,\alpha\beta-\alpha\beta} = -6.5k_BT$. 20 simulations each

were performed at tubulin concentration 2-20μM. MT growth speed was obtained from each MT length versus time trace and overlaid on experimental data. (B) MT nucleation from γ-TuRC was simulated with input polymerization parameters defined above, $\Delta G_{\gamma TuRC-conf} = 10 k_B T$ and $\Delta G_{Long,\gamma-\alpha\beta} = 1.1\Delta G_{Long,\alpha\beta-\alpha\beta}$. $k_{\gamma TuRC-conf}$ was varied from $(1 - 0.001)s^{-1}$. Tubulin concentration was varied from 5-30μM. 200 simulations were performed for a given tubulin concentration at every $k_{\gamma TuRC-conf}$ value, except for $k_{\gamma TuRC-conf} = 0.01s^{-1}$ where 500 simulations were performed. Probability of MT nucleation ($p(t)$) versus time (t) curves at 15μM tubulin are displayed in (i). The initial rate of nucleation $\frac{dp}{dt}\Big|_{t\to 0}$ was measured and plotted against concentration on a log-log axis in (ii). The critical nucleus size does not change significantly while the absolute rate of nucleation decreases with decreasing $k_{\gamma TuRC-conf}$. (C) MT nucleation from γ-TuRC was simulated with input polymerization parameters defined above, $\Delta G_{\gamma TuRC-conf} = 10 k_B T$ and $k_{\gamma TuRC-conf} = 0.01s^{-1}$. $\Delta G_{Long,\gamma-\alpha\beta}$ was varied from $(0.7 - 1.3) \times \Delta G_{Long,\alpha\beta-\alpha\beta}$. 200 simulations were performed for every $\Delta G_{Long,\gamma-\alpha\beta}$ value at tubulin concentrations between 2.5-30μM, except for $\Delta G_{Long,\gamma-\alpha\beta} = 1.1\Delta G_{Long,\alpha\beta-\alpha\beta}$ where 500 simulations were performed. Probability of MT nucleation ($p(t)$) versus time (t) curves at 20μM tubulin are displayed in (i). The initial rate of nucleation $\frac{dp}{dt}\Big|_{t\to 0}$ was measured and plotted against concentration on a log-log axis in (ii). For $0.7, 0.9, 1.3\Delta G_{Long,\alpha\beta-\alpha\beta}$, either few MTs nucleate or nucleation occurs immediately, and critical nucleus size could not be accurately measured. See also Figure 5.

Figure 5-figure supplement 2. Simulations of microtubule nucleation from γ-TuRC and from blunt seeds.

(A) Simulations recapitulated experimental data for γ-TuRC-mediated MT nucleation. Parameter values used: $k_{on} = 1.3 \times 10^6\ (M^{-1}s^{-1}pf^{-1})$, $\Delta G_{Long,\alpha\beta-\alpha\beta} = -7.2k_BT$, $\Delta G_{Lat,\alpha\beta-\alpha\beta} = -6.5k_BT$, $\Delta G_{Long,\gamma-\alpha\beta} = 1.1\Delta G_{Long,\alpha\beta-\alpha\beta}$, $k_{\gamma TuRC-conf} = 0.01s^{-1}$ and $\Delta G_{\gamma TuRC-conf} = 10k_BT$. 500 simulations each were performed for a range of tubulin concentration 5-25μM. Probability of MT nucleation ($p(t)$) versus time (t) is displayed in (i). The initial rate of nucleation $\left.\frac{dp}{dt}\right|_{t\to 0}$ was measured at each tubulin concentration and plotted against concentration on a log-log axis in (ii). Linear curve was fit for n=5 simulated data points, and critical nucleus of 4 ± 0.4 αβ-tubulins. See Figure 2C-D for comparison with experimental results. (B) MT nucleation dynamics from a closed γ-TuRC were simulated to compare with experimental data for blunt-seed mediated MT assembly. Parameter values used: $k_{on} = 1.3 \times 10^6\ (M^{-1}s^{-1}pf^{-1})$, $\Delta G_{Long,\alpha\beta-\alpha\beta} = -7.2k_BT$, $\Delta G_{Lat,\alpha\beta-\alpha\beta} = -6.5k_BT$, $\Delta G_{Long,\gamma-\alpha\beta} = 1.0\Delta G_{Long,\alpha\beta-\alpha\beta}$. An input for $k_{\gamma TuRC-conf}$ or $\Delta G_{\gamma TuRC-conf}$ were not required because γ-TuRC does not undergo an open-to-closed transition. 200 simulations each were performed for a range of tubulin concentration 2-8μM. For each simulation, time point where over 50nm length of MT has assembled was recorded. Probability of MT nucleation ($p(t)$) versus time (t) is displayed in (i). The initial rate of nucleation $\left.\frac{dp}{dt}\right|_{t\to 0}$ was measured at each tubulin concentration and plotted against concentration, C-C* on a log-log axis in (ii). Critical concentration of polymerization, C*=1.4μM. Linear curve was fit for n=7 simulated data points, and critical nucleus of 1.1 ± 1 αβ-tubulins. See Figure 3D-E for comparison with experimental results. See also Figure 5.

Figure 6-figure supplement 1. Effect of putative activation factor NME7 on γ-TuRC-mediated nucleation.

(A) A constant density of γ-TuRC molecules were attached without (left) and with (right) 6μM NME7 and 10.5μM tubulin ± 1μM additional NME7 was added. Experiments were repeated twice on different experimental days with the same γ-TuRC preparation. See also Figure 6 and Video 6.

Figure 7-figure supplement 1. Role of XMAP215 on γ-TuRC-mediated microtubule nucleation.

(A) γ-TuRCs were attached and 3.5-7μM tubulin ± 20nM XMAP215-GFP was added. Experiment was repeated identically two times with independent γ-TuRC purifications. One additional replicated was performed with 7μM tubulin. (B) Number of MTs nucleated ($N(t)$) over time (t) is plotted and shaded regions represent 95% confidence interval $(n \pm 2\sqrt{n})$ in the number of nucleated MTs (n) assuming a Poisson distribution as described in Methods. Analyses were repeated twice with independent γ-TuRC purifications, and representative dataset is reported to highlight the absolute increase in the number of MTs nucleated by XMAP215. One additional supporting replicate was obtained only at 7μM tubulin. (C) Titrating tubulin with constant γ-TuRC and XMAP215 concentration. XMAP215/γ-TuRC molecules were observed to nucleate MTs at low tubulin concentrations of 1.6-3.5μM. Experiments were repeated at three times with independent γ-TuRC preparations, and fewer concentration points were repeated another two times. (D) The role of C-terminal region of XMAP215 or N-terminal region was tested in the cooperative nucleation with purified γ-TuRC. MTs nucleated by γ-TuRC alone (top-left panel), γ-TuRC with 20nM full-length XMAP215 (top-right panel), γ-TuRC with 20nM C-terminal domain containing TOG5 and C-terminus of XMAP215 (bottom-left panel), or γ-TuRC with 20nM N-terminal domain containing TOG1-4 domains (bottom-right). While the N-terminus is not sufficient for MT nucleation, C-terminal domain of XMAP215, which binds γ-TuRC directly, also

1490 does not stimulate MT nucleation from γ-TuRC. (E) MT nucleation was measured, and number of
1491 MTs nucleated with wild-type XMAP215 reactions at 150 seconds was set to 1 to account for
1492 variable γ-TuRC concentration across purifications. Individual dataset with ±wt XMAP215,
1493 TOG5-CT or TOG1-4 are reported with solid, dashed or dotted curves. The number of times the
1494 experiment in (D-E) was repeated independent γ-TuRC preparations is as follows: buffer (3), wild-
1495 type XMAP215 (3), TOG1-4 (2), TOG5-CT (2). All data was pooled and reported in (E). Shaded
1496 regions represent 95% confidence interval $(n \pm 2\sqrt{n})$ in the number of nucleated MTs (n)
1497 assuming a Poisson distribution as described in Methods. Scale bars, 10μm. See also Figure 7 and
1498 Videos 7-8.
1499
1500 **Figure 7-figure supplement 2. MCAK and Stathmin inhibit γ-TuRC-mediated nucleation.**
1501 (A) γ-TuRC molecules were attached to coverslips and either 10.5μM tubulin alone (left panels),
1502 10μM tubulin + 10nM MCAK (top-right) or 10μM tubulin + 5μM Stathmin (bottom-right) was
1503 added to the reaction. Both MCAK and Stathmin were observed to decrease the number of MTs
1504 nucleated. For MCAK, the experiment and control were repeated three times with independent γ-
1505 TuRC preparations. For Stathmin, the experiment and control were repeated identically two times
1506 with independent γ-TuRC preparations and an additional, supporting experiment was performed
1507 at a slightly different concentration (7μM tubulin ± 2μM Stathmin). See also Figure 7 and Video
1508 9.

Video Legends

Video 1. Microtubule nucleation from γ-TuRC complexes

γ-TuRC was attached to functionalized coverslips and MT nucleation was observed upon introducing fluorescent αβ-tubulin (gray). MTs nucleated from individual γ-TuRC molecules from zero length at 14μM αβ-tubulin and the plus-end of nucleated MTs polymerized, but not its minus-end. Elapsed time is shown in seconds, where time-point zero represents the start of reaction. Scale bar, 10 μm.

Video 2. Microtubule nucleation from fluorescent, single γ-TuRC molecules

Alexa-568 labelled γ-TuRC (green) was attached to functionalized coverslips and MT nucleation was observed upon introducing fluorescent αβ-tubulin (red). MTs nucleated from single γ-TuRC molecules at 10.5μM αβ-tubulin. Elapsed time is shown in seconds, where time-point zero represents the start of reaction. Scale bar, 10 μm.

Video 3. γ-TuRC molecules nucleate microtubules efficiently

Constant density of γ-TuRC was attached while concentration of fluorescent αβ-tubulin was titrated (3.5-21μM) and MT nucleation was observed. γ-TuRC molecules nucleated MTs starting from 7μM tubulin and MT nucleation increased non-linearly with increasing tubulin concentration. Elapsed time is shown in seconds, where time-point zero represents the start of reaction. Scale bar, 10 μm.

Video 4. Spontaneous microtubule nucleation occurs at high tubulin concentration

Concentration of fluorescent αβ-tubulin was titrated (7-21μM) and spontaneous MT nucleation was assayed. MTs nucleated spontaneously starting from high concentration of 14μM tubulin and MT nucleation increased non-linearly with tubulin concentration. Both plus- and minus-ends of the assembled MTs polymerize. Elapsed time is shown in seconds, where time-point zero represents the start of reaction. Scale bar, 10 μm.

Video 5. Microtubule assembly from blunt plus-ends resembles polymerization

MTs with blunt ends (seeds, cyan) were generated and attached to functionalized coverslips. Varying concentration of fluorescent αβ-tubulin was added (1.4-8.7μM, pseudo-colored as magenta) and MT assembly from seeds was assayed. MTs assembled at concentration above 1.4μM tubulin, which is the minimum concentration needed for polymerization of MT plus-ends (*C**). Elapsed time is shown in seconds, where time-point zero represents the start of reaction. Scale bar, 10 μm.

Video 6. γ-TuNA motif from CDK5RAP2, NME7 and TPX2 do not significantly increase γ-TuRC-mediated microtubule nucleation

Top panels: γ-TuRC was immobilized on coverslips with control buffer (left) or with 6μM γ-TuNA motif from CDK5RAP2 (right) and MT nucleation was observed upon introducing fluorescent 10.5μM αβ-tubulin (gray) without or with 3μM γ-TuNA, respectively.

Middle panels: γ-TuRC was immobilized on coverslips with control buffer (left) or with 6μM NME7 (right) and MT nucleation was observed upon introducing fluorescent 10.5μM αβ-tubulin (gray) without or with 1μM NME7, respectively.

Bottom panels: γ-TuRC was immobilized on coverslips and MT nucleation was observed upon introducing fluorescent 10.5μM αβ-tubulin (pseudo-colored as red) without or with 10nM GFP-TPX2 (right, labelled as green). TPX2 bound along the nucleated MTs but did not significantly increase the MT nucleation activity of γ-TuRC molecules.

Elapsed time is shown in seconds, where time-point zero represents the start of reaction. Scale bar, 10 μm.

Video 7. XMAP215 increases microtubule nucleation activity of γ-TuRC

γ-TuRC was immobilized on coverslips and MT nucleation was assayed with low concentration of fluorescent αβ-tubulin (3.5μM and 7μM) without (top panels) or with 20nM XMAP215-GFP (bottom panels). XMAP215 induces MT nucleation from γ-TuRC. Elapsed time is shown in seconds, where time-point zero represents the start of reaction. Scale bar, 10 μm.

Video 8. Synergistic microtubule nucleation by γ-TuRC and XMAP215

Triple-color fluorescence microscopy was performed to observe the molecular sequence of events during MT nucleation from γ-TuRC and XMAP215. γ-TuRC (blue) and XMAP215 (red) formed a complex before MT nucleation occurred (pseudo-colored as green). For 50% of these events, XMAP215 remains on the nucleated minus-end. Elapsed time is shown in seconds, where time-point zero represents the start of reaction. Scale bar, 10 μm.

Video 9. MCAK and Stathmin inhibit γ-TuRC-mediated microtubule nucleation

Top panels: γ-TuRC was immobilized on coverslips and MT nucleation was observed upon introducing fluorescent 10.5μM αβ-tubulin without (left) or with 10nM MCAK (right).

Bottom panels: γ-TuRC was immobilized on coverslips and MT nucleation was observed upon introducing fluorescent 10.5μM αβ-tubulin without (left) or with 5μM Stathmin (right). Elapsed time is shown in seconds, where time-point zero represents the start of reaction. Scale bar, 10 μm.

Source Data files.

Figure 2-Source Data 1. Source data for Figure 2B-D. Each excel sheet is labelled with individual figure panel. For Figure 2C, all three experimental replicates are supplied, and dataset 1 is plotted.

Figure 3-Source Data 1. Source data for Figure 3 panels B, D, E and Figure 3-supplement 1C-D. Each excel sheet is labelled with individual figure panel. For Figure 3D, all three experimental replicates are supplied, and dataset 1 is plotted.

Figure 4-Source Data 1. Source data for Figure 4C.

Figure 6-Source Data 1. Source data for Figure 6 panels B, D.

Figure 7-Source Data 1. Source data for Figure 7 panels B, D, E, F and Figure 7-supplement 1 panels B, E. Each excel sheet is labelled with individual figure panel. For Figure 7D, all five experimental replicates are supplied, and dataset 1 is plotted.

Source Code.

MATLAB code for Monte Carlo simulations used to model the dynamics of γ-TuRC-mediated nucleation. Methods section details how the simulation was set up and performed. Figure 6-supplements 2 provide the parameters used to model our experimental data.

Figure 1

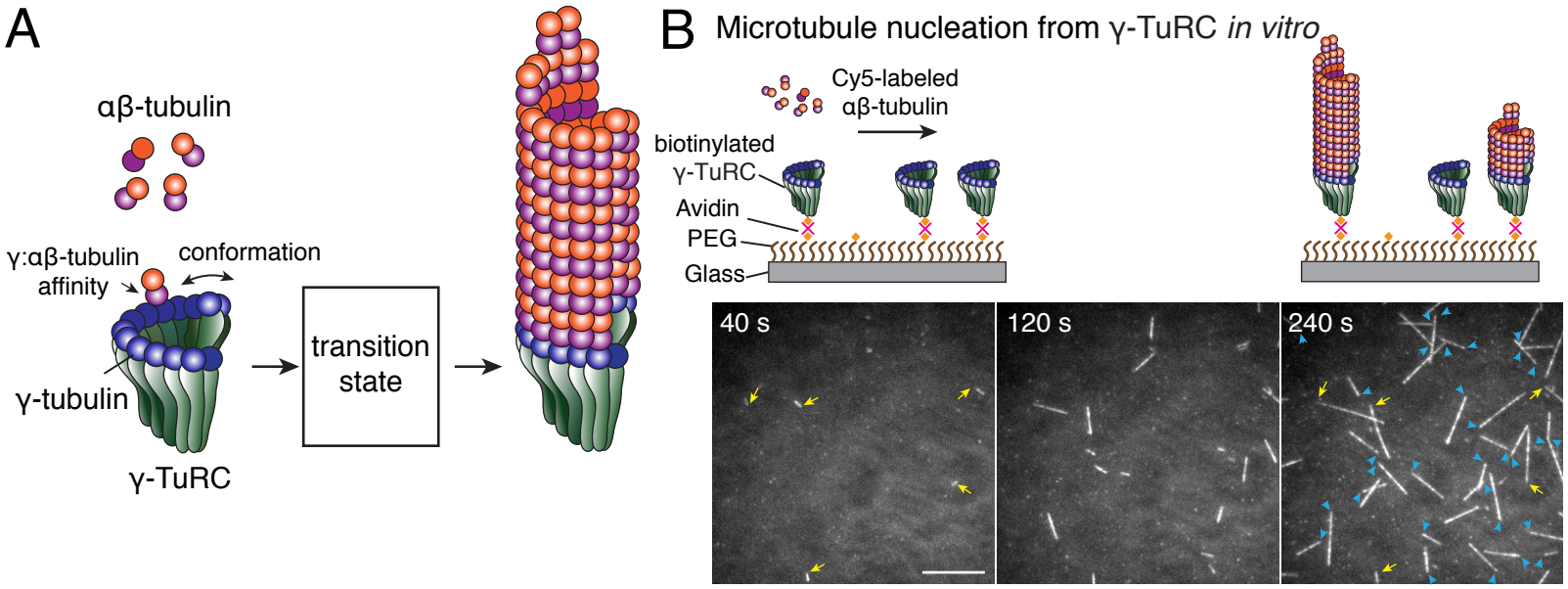

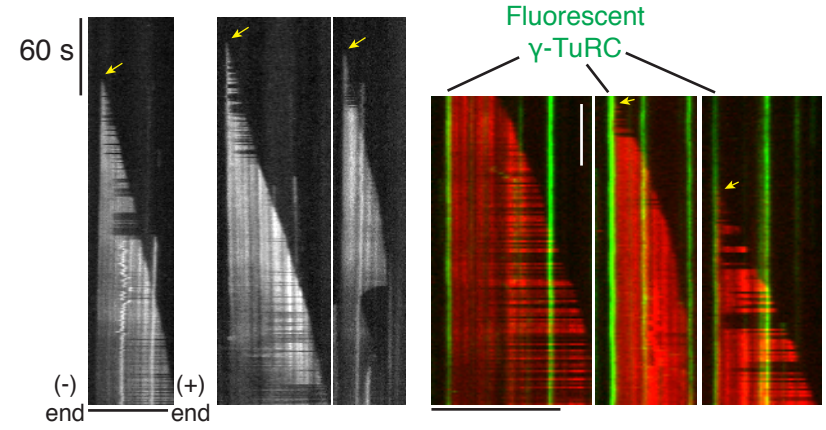

Figure 1-figure supplement 1

γ-TuRC purification and quality control reactions

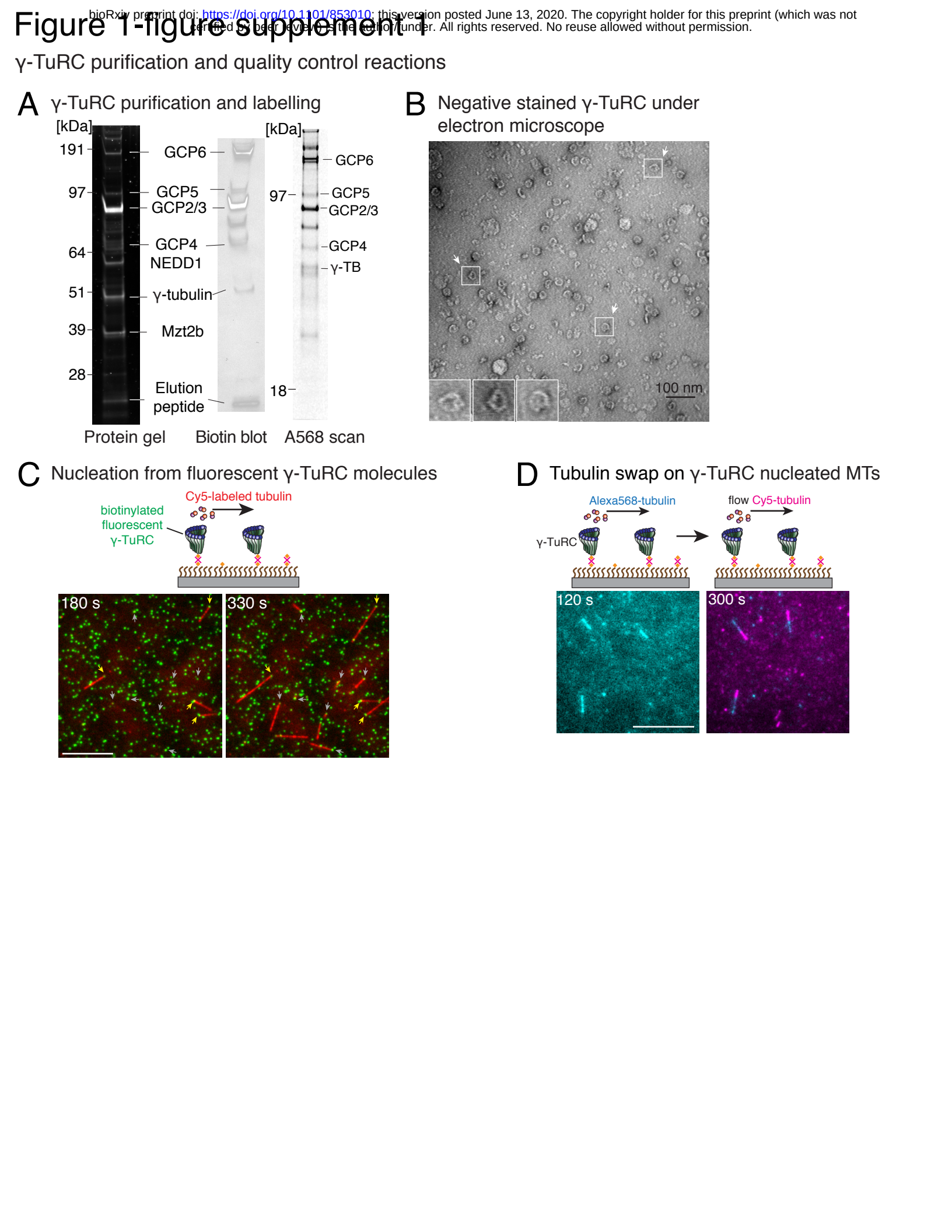

Figure 2

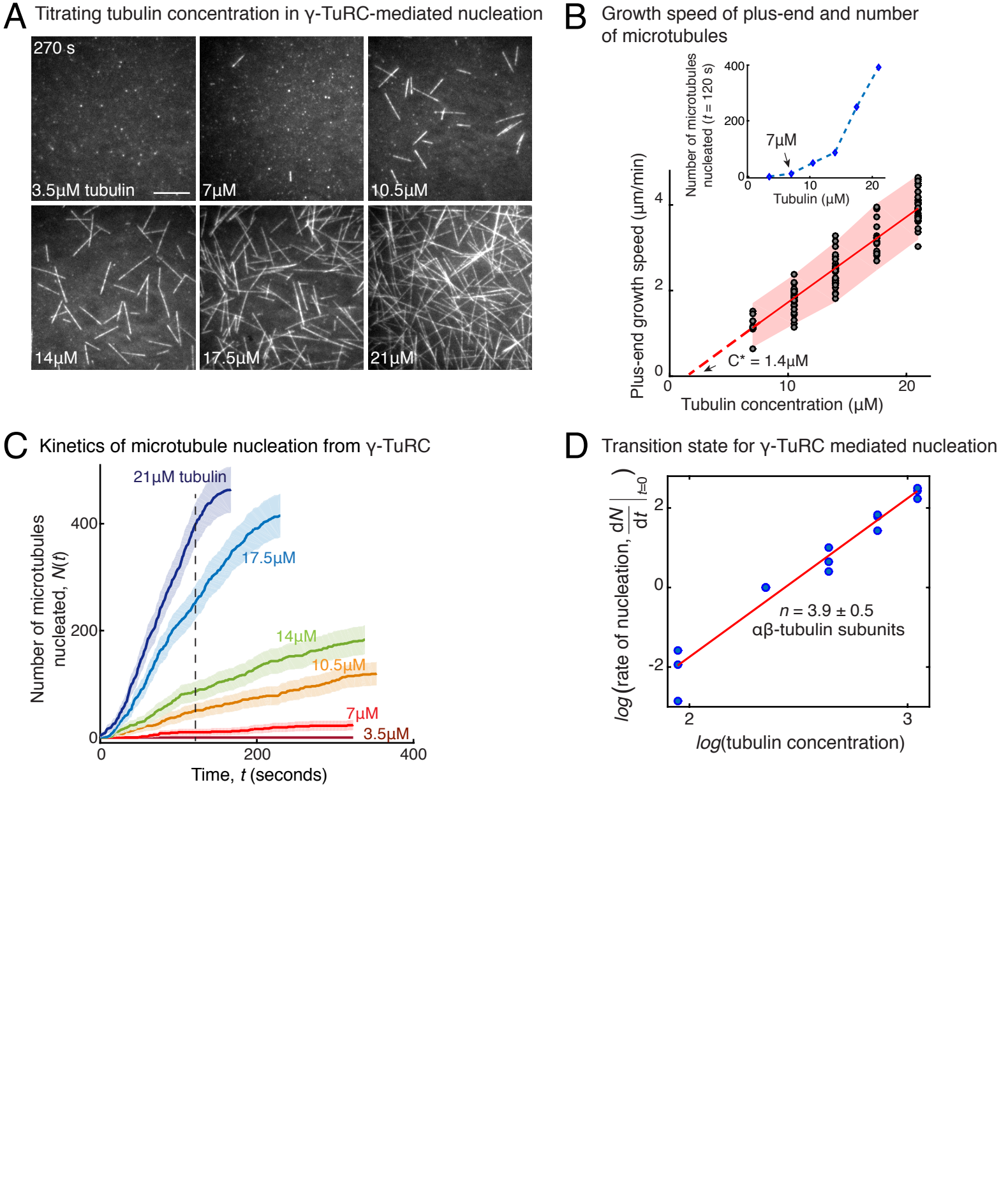

Figure 3

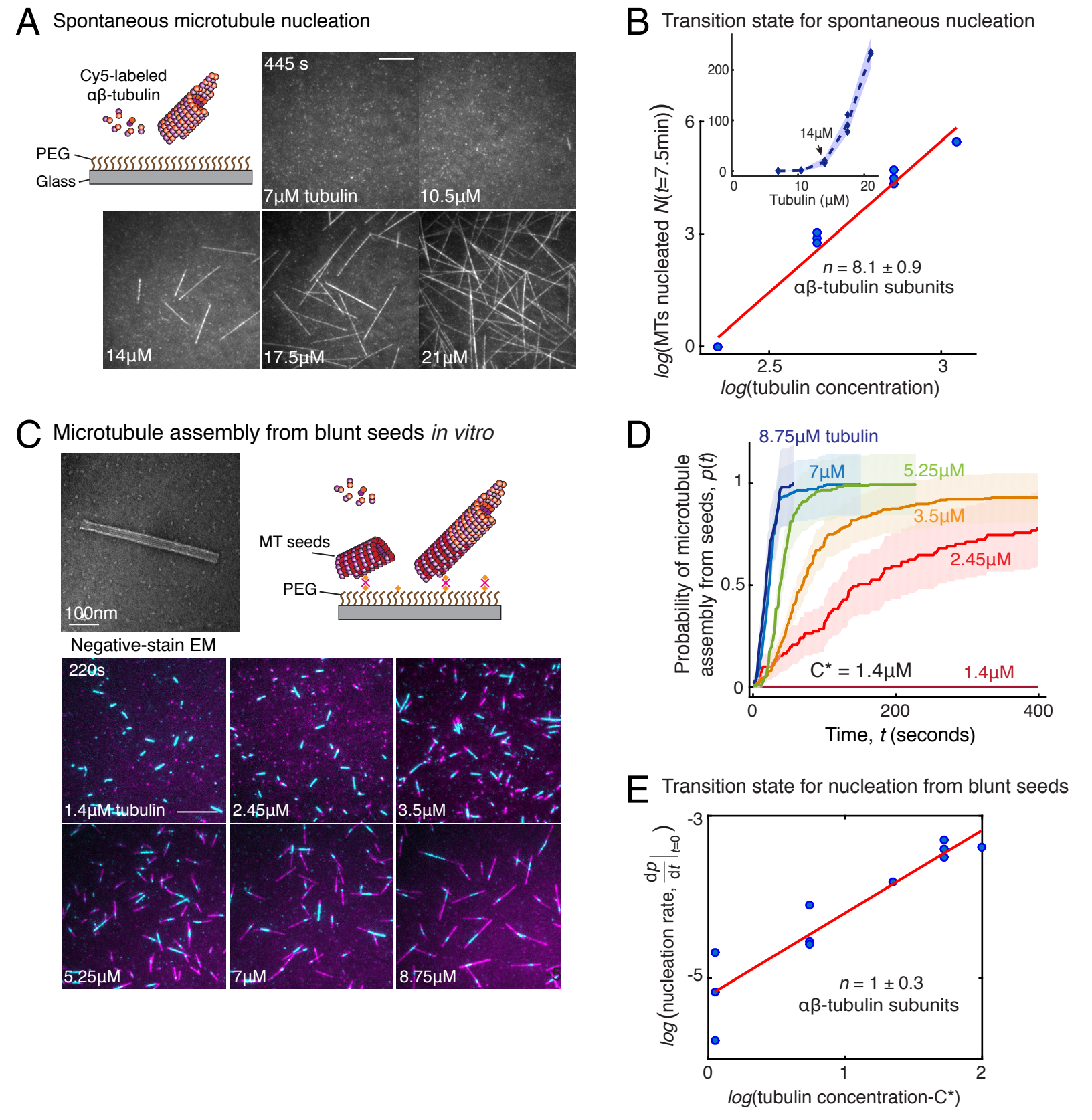

Figure 4

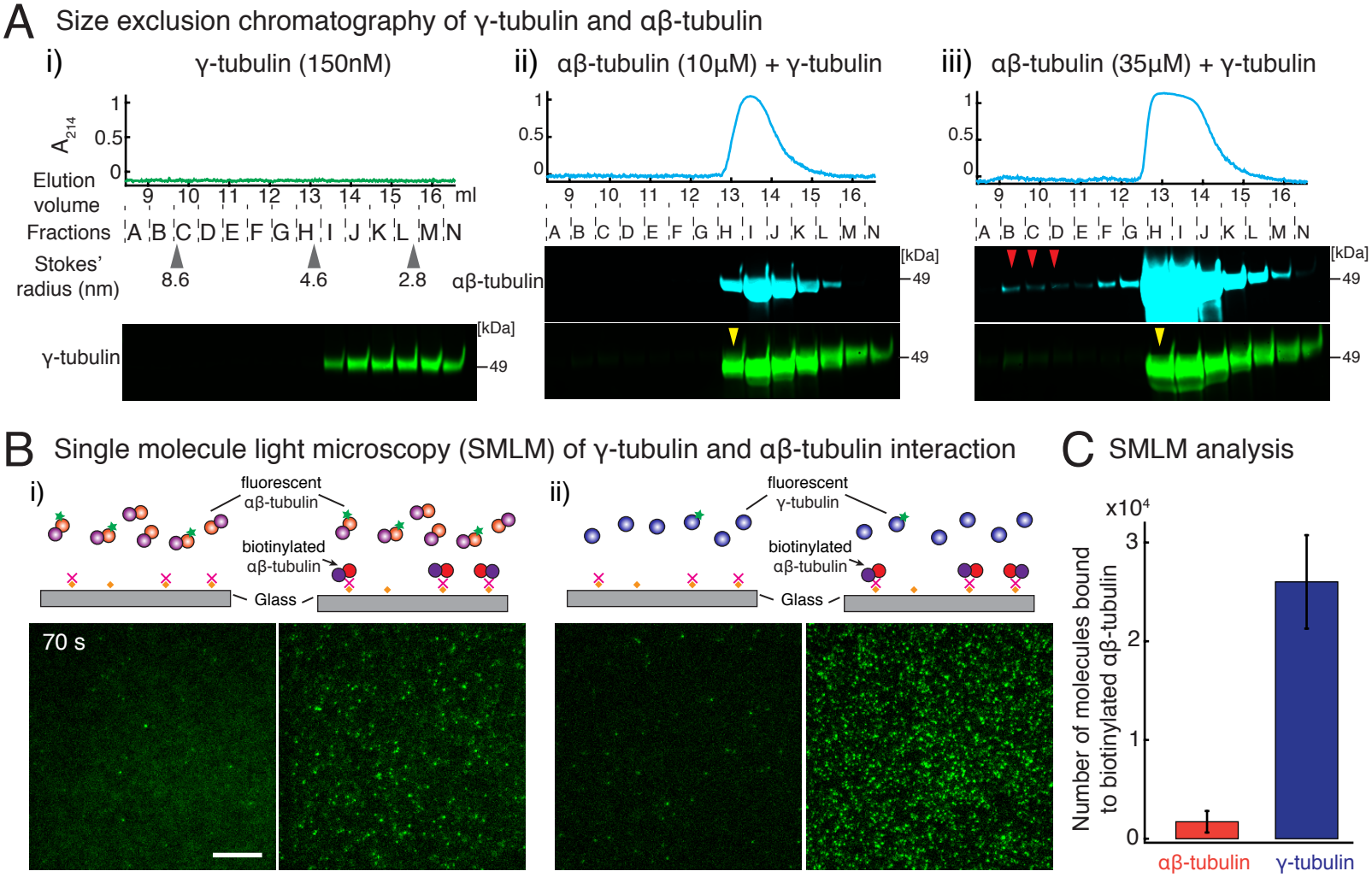

Figure 3-figure supplement 1

Comparison of γ-TuRC-mediated and spontaneous nucleation

A Kymographs of spontaneously nucleated MTs

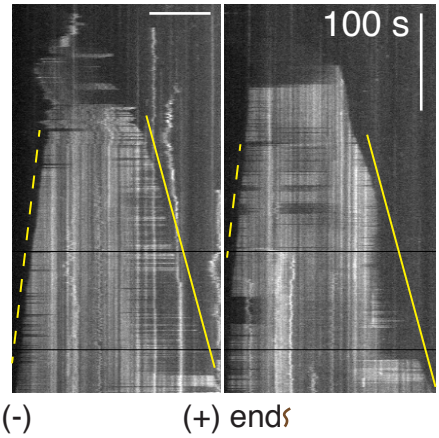

B γ-TuRC-mediated versus spontaneous nucleation and control reactions

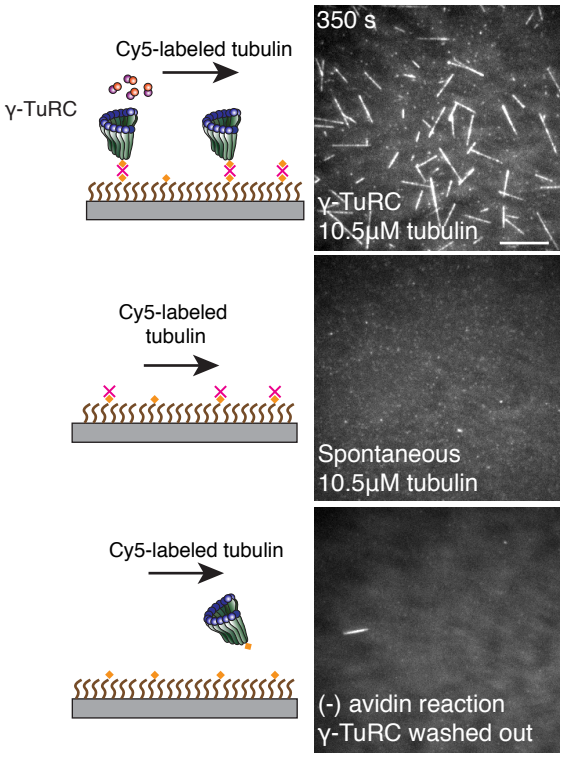

C Nucleation kinetics from γ-TuRCs versus spontaneous assembly

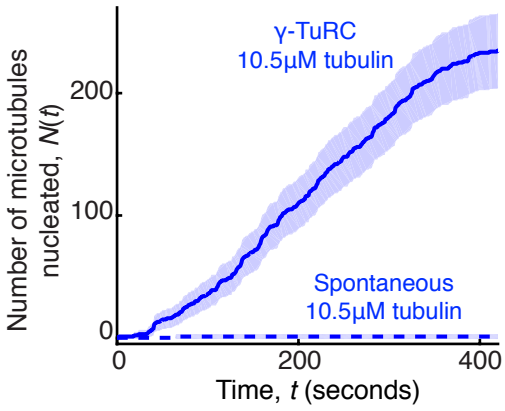

Growth speed of microtubule plus-ends assembled from blunt seeds and γ-TuRCs

D

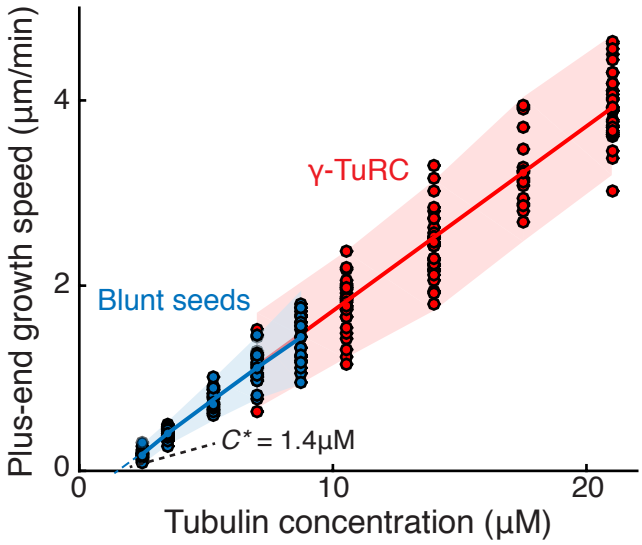

Figure 4

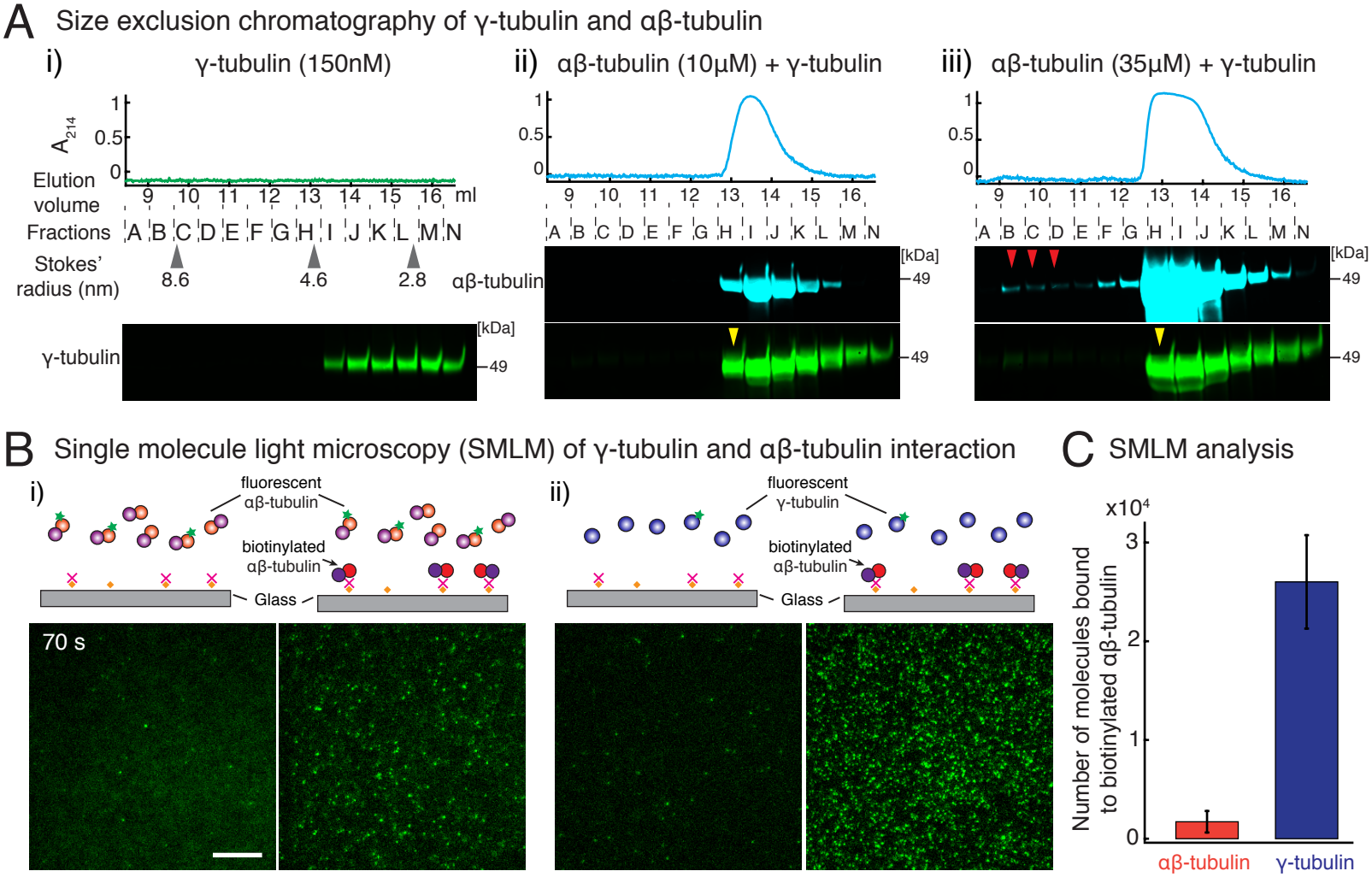

Figure 4-figure supplement 1

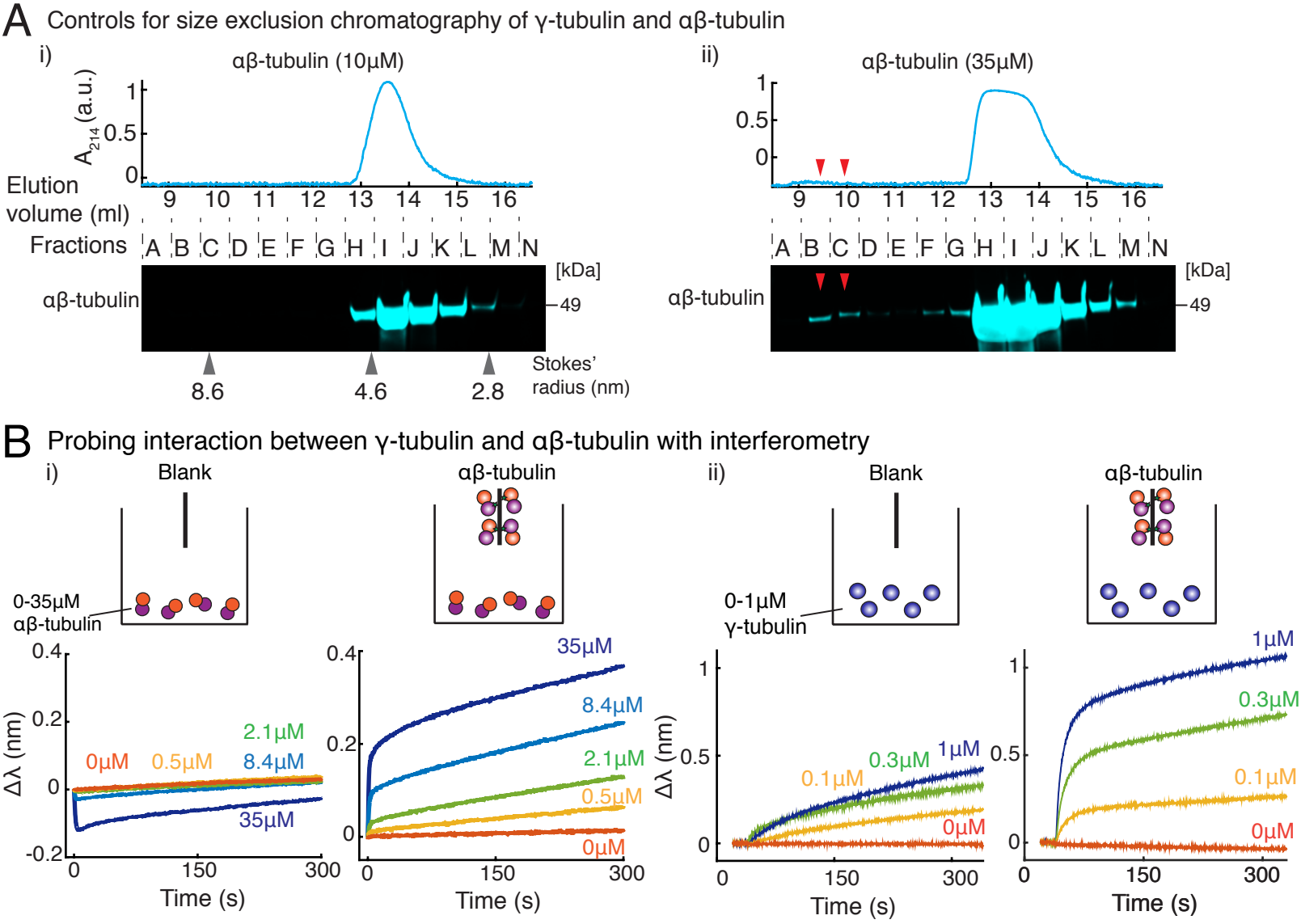

Figure 4-figure supplement 2

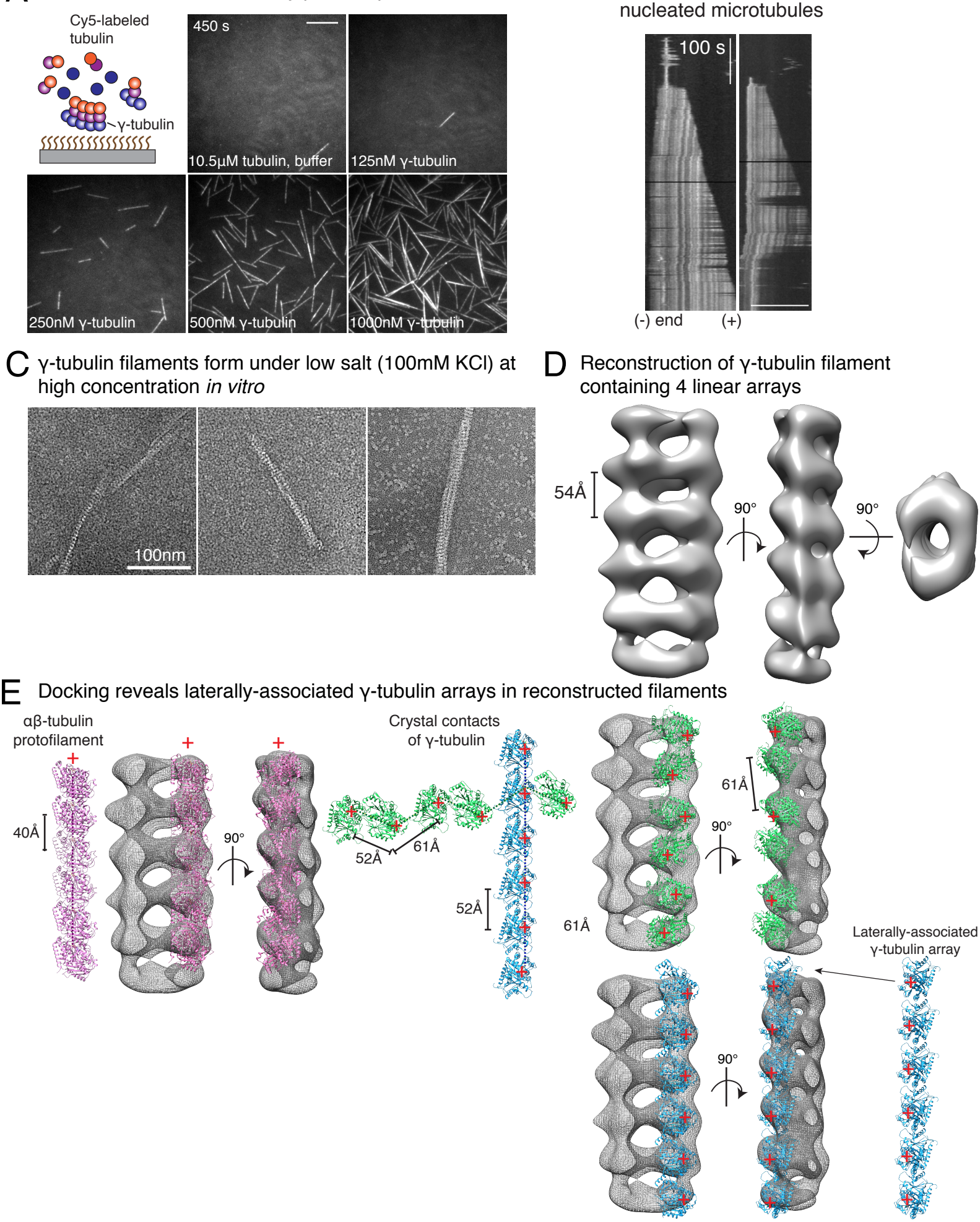

Figure 5

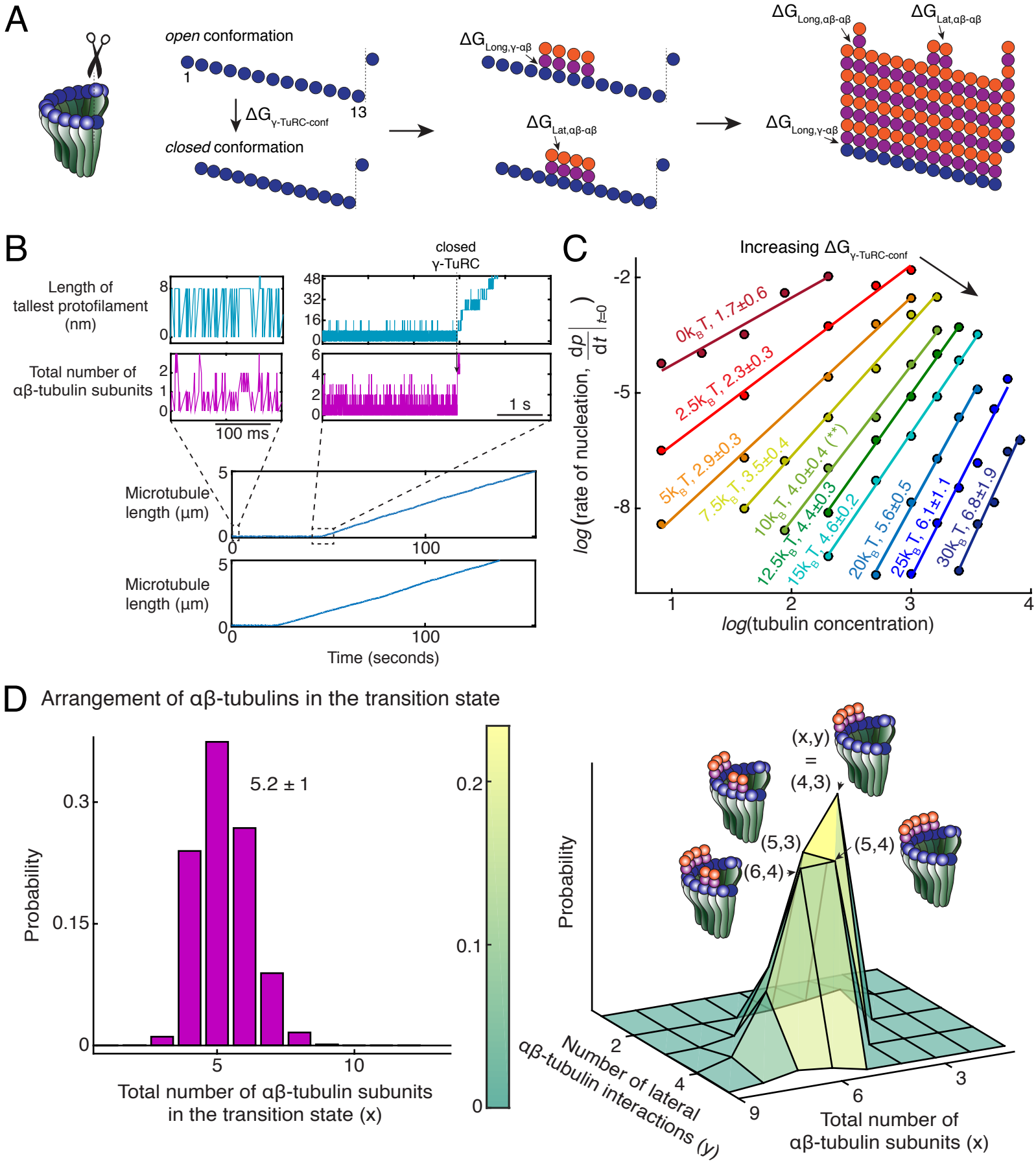

Figure 5-figure supplement 1

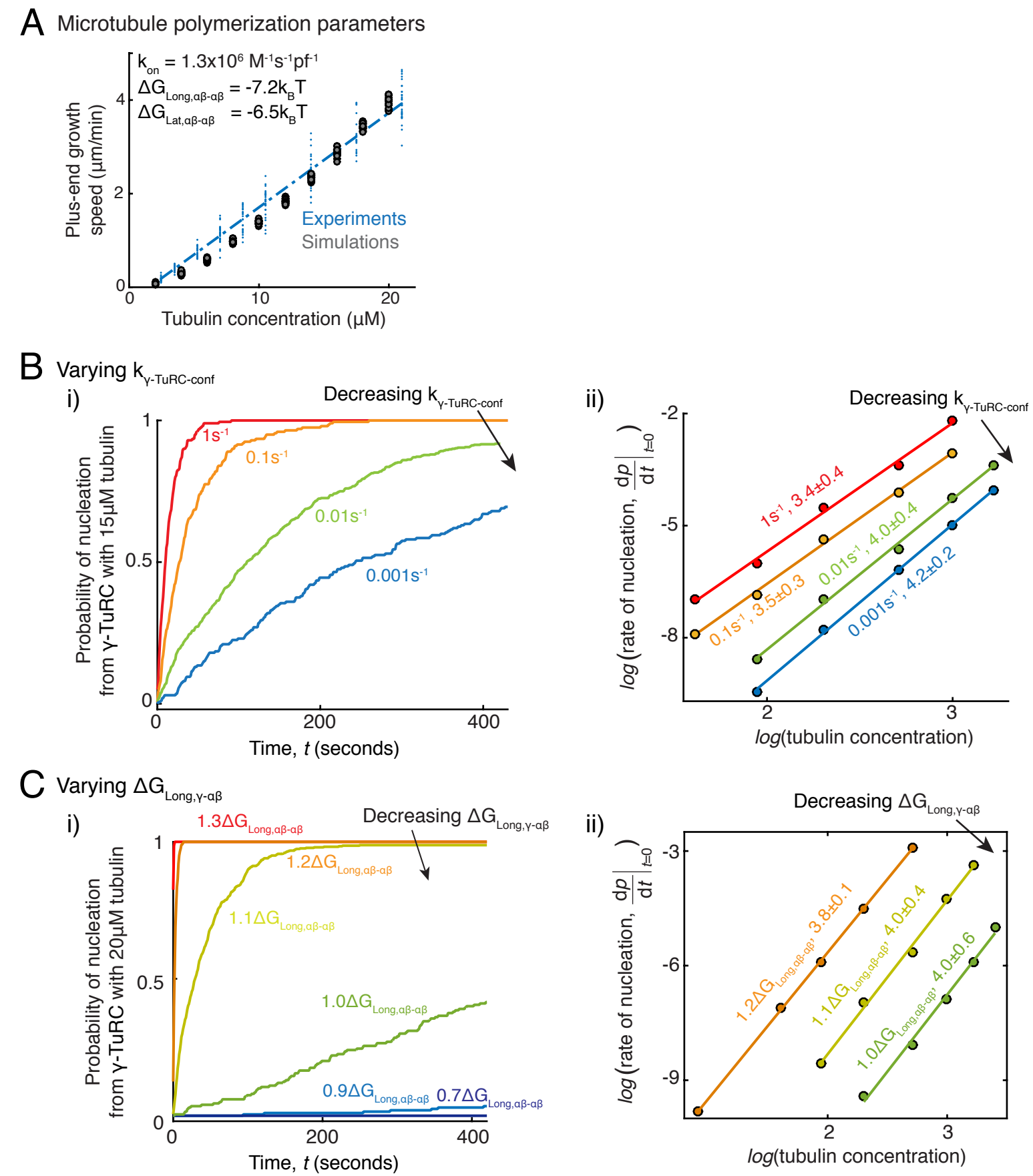

Figure 5-figure supplement 2

A Simulated kinetics of microtubule nucleation from γ-TuRC

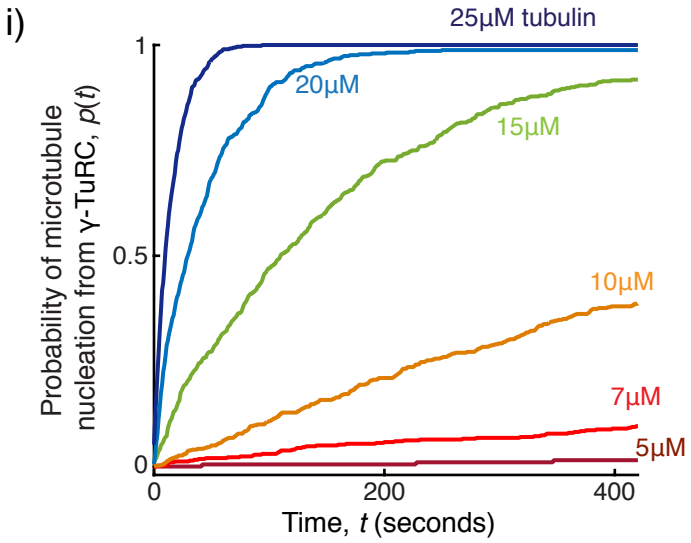

B Simulated kinetics of nucleation from *closed* γ-TuRC conformation

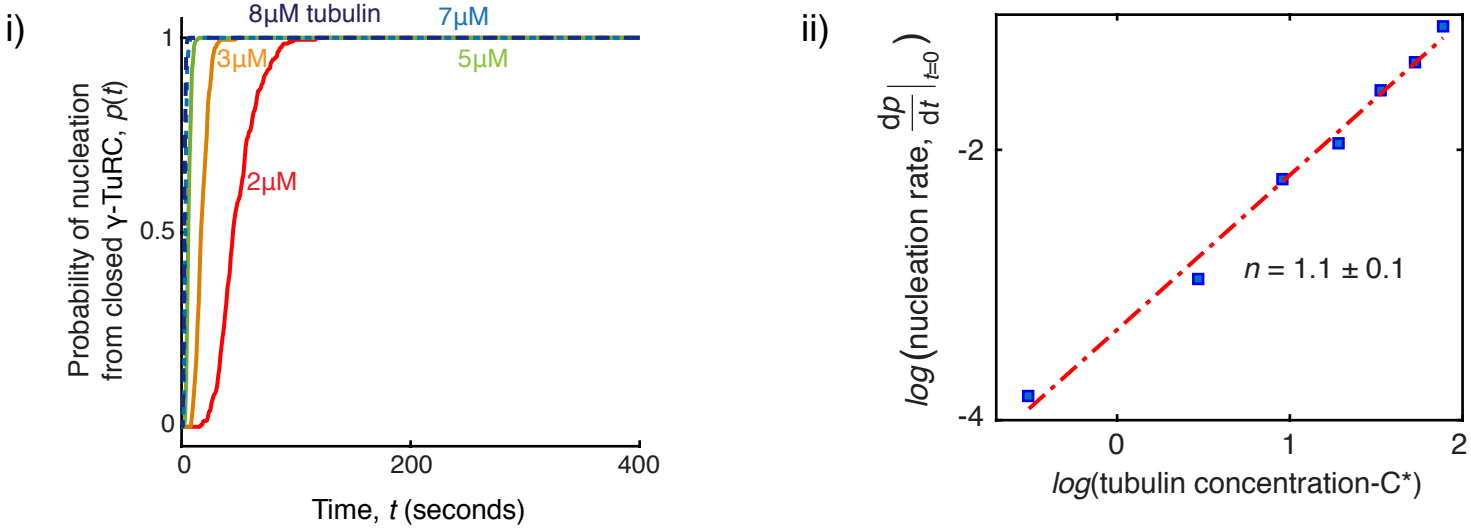

Figure 6

A Addition of activation factors to γ-TuRC

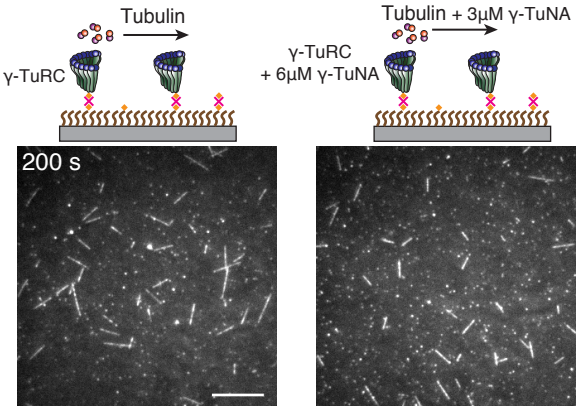

B γ-TuNA and NME7 have a minor effect on γ-TuRC-mediated nucleation

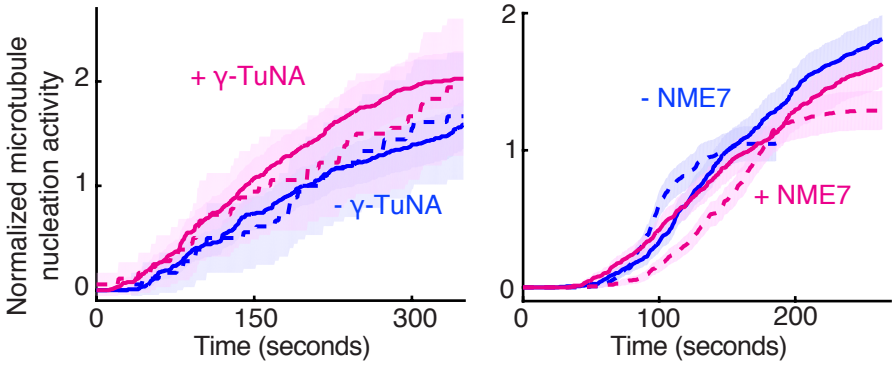

C Addition of TPX2 to γ-TuRC-mediated nucleation

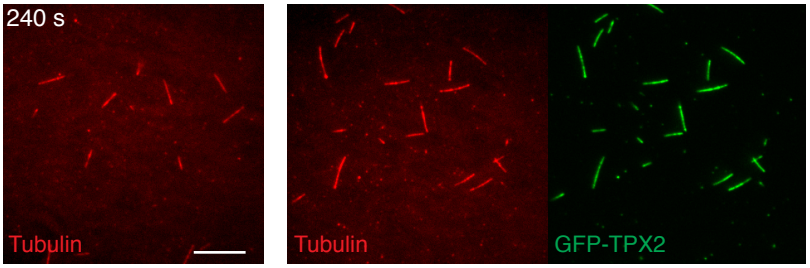

γ-TuRC +
10.5μM tubulin

γ-TuRC +
10.5μM tubulin + 10-20nM GFP-TPX2

D TPX2 has a small effect on γ-TuRC's nucleation activity

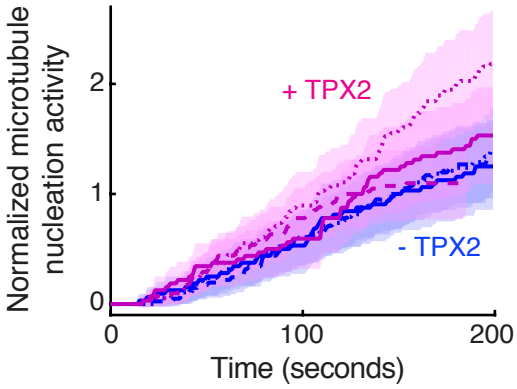

Figure 6-figure supplement 1

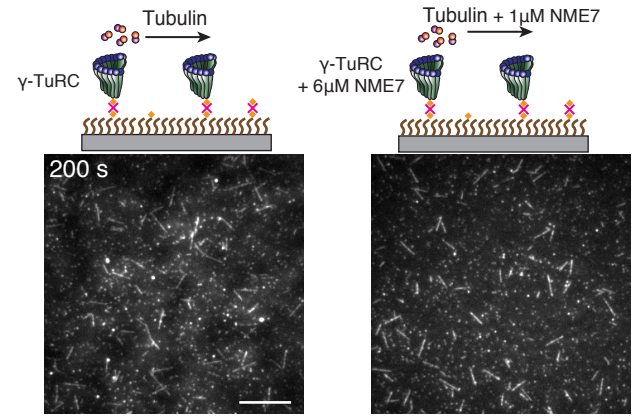

Figure 7

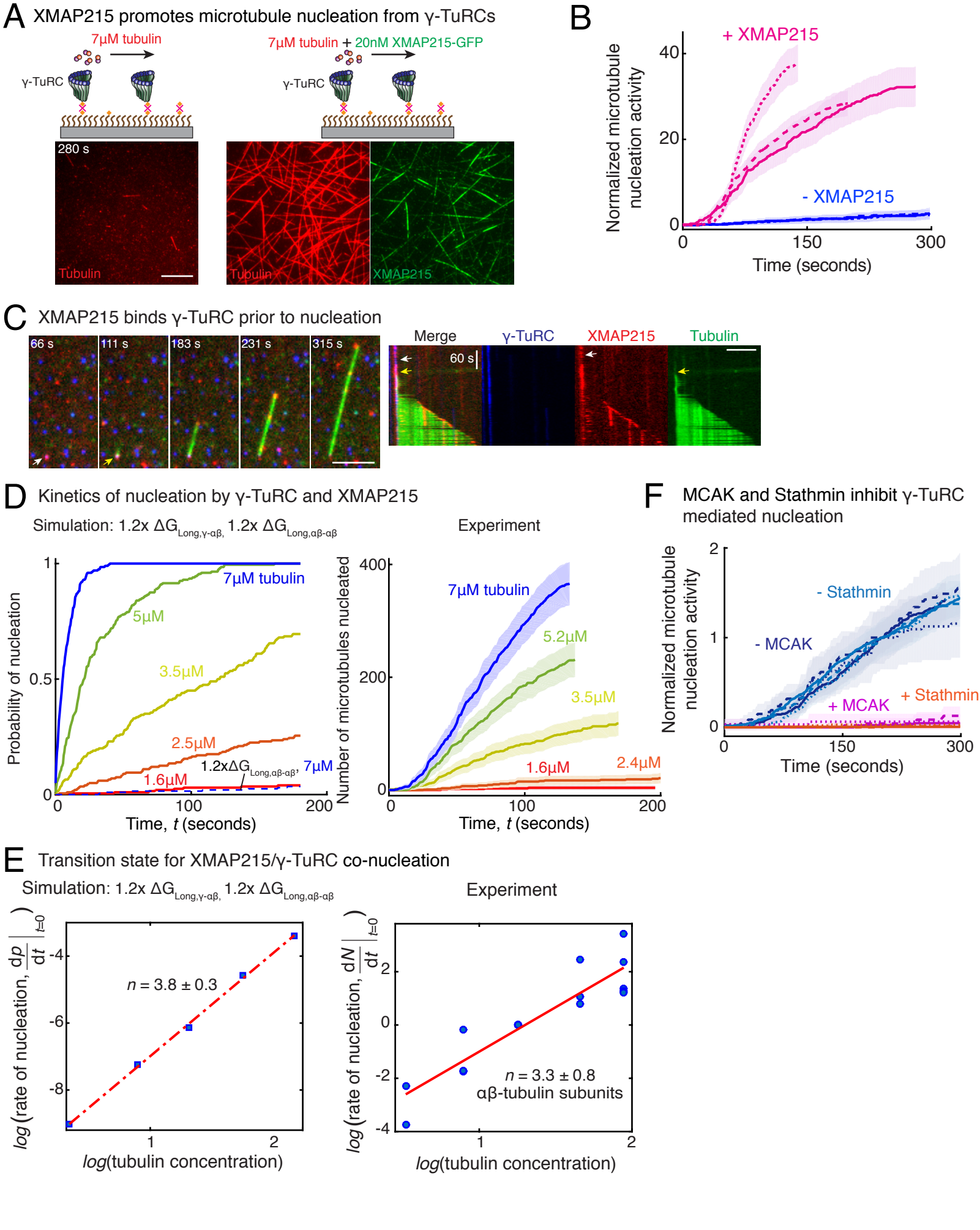

Figure 7-figure supplement 1

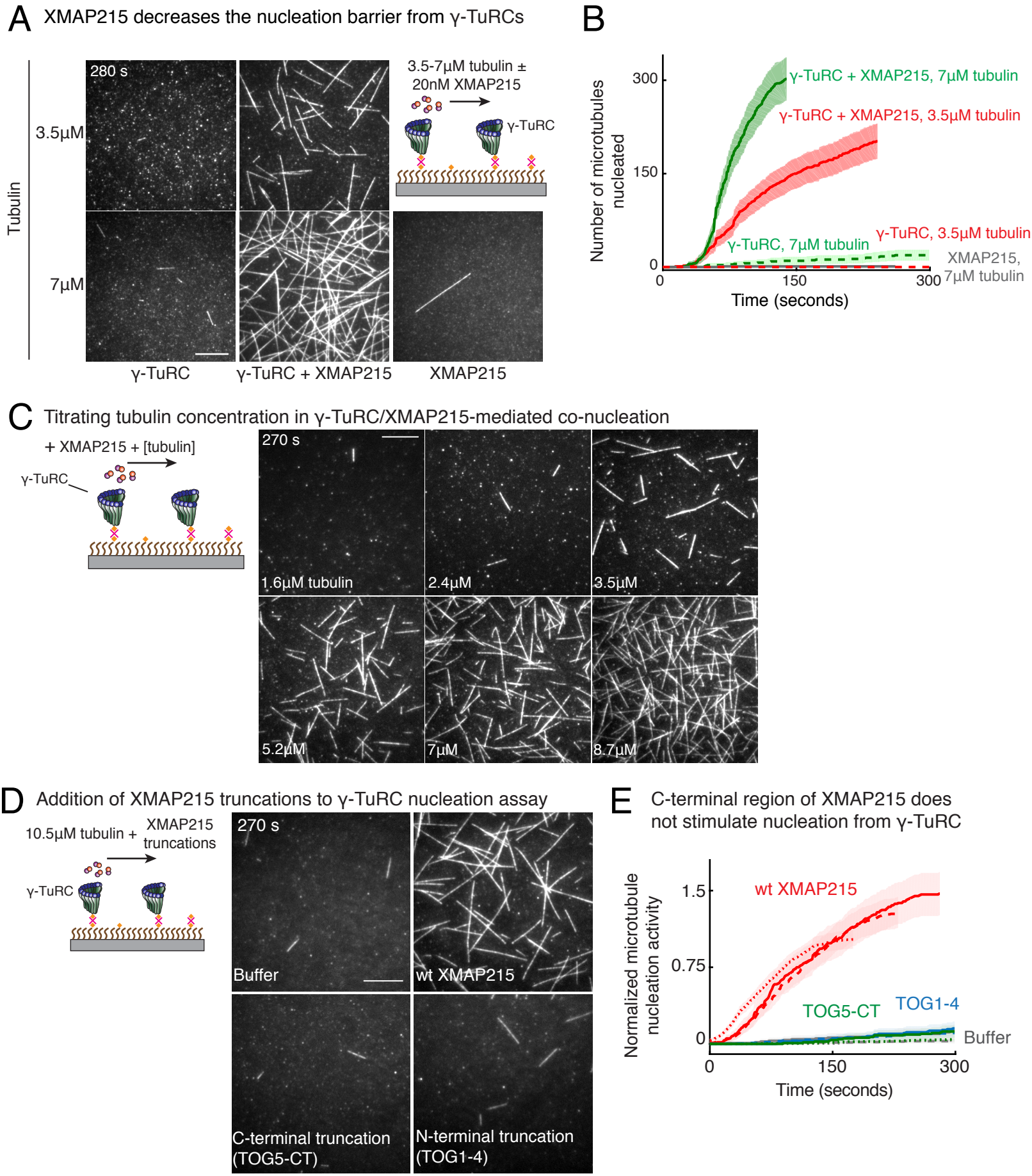

Figure 7-figure supplement 2